DOI: 10.1002/chem.200902741

Stable Anticancer Gold(III)–Porphyrin Complexes: Effects of Porphyrin Structure

Raymond Wai-Yin Sun, Carrie Ka-Lei Li, Dik-Lung Ma, Jessie Jing Yan, Chun-Nam Lok, Chung-Hang Leung, Nianyong Zhu, and Chi-Ming Che*[a]

Abstract: In the design of physiologically stable anticancer gold(III) complexes, we have employed strongly chelating porphyrinato ligands to stabilize a gold(III) ion [*Chem. Commun*. **2003**, 1718; *Coord. Chem. Rev.* **2009**, *253*, 1682]. In this work, a family of gold(III) tetraarylporphyrins with porphyrinato ligands containing different peripheral substituents on the *meso*-aryl rings were prepared, and these complexes were used to study the structure–bioactivity relationship. The cytotoxic IC_{50} values of $[Au(Por)]^+$ (Por = porphyrinato ligand), which range from 0.033 to >100 μM, correlate with their lipophilicity and cellular uptake. Some of them induce apoptosis and display preferential cytotoxicity toward cancer cells than to normal noncancerous cells. A new gold(III)–porphyrin with saccharide conjugation [Au(4-glucosyl-TPP)]Cl (**2a**; H_2(4-glucosyl-TPP) = *meso*-tetrakis(4-β-D-glucosylphenyl)-porphyrin) exhibits significant cytostatic activity to cancer cells ($IC_{50} = 1.2$–9.0 μM) without causing cell death and is much less toxic to lung fibroblast cells ($IC_{50} > 100$ μM). The gold(III)–porphyrin complexes induce S-phase cell-cycle arrest of cancer cells as indicated by flow cytometric analysis, suggesting that the anticancer activity may be, in part, due to termination of DNA replication. The gold(III)–porphyrin complexes can bind to DNA in vitro with binding constants in the range of 4.9×10^5 to 4.1×10^6 dm^3mol^{-1} as determined by absorption titration. Complexes **2a** and $[Au(TMPyP)]Cl_5$ (**4a**; $[H_2TMPyP]^{4+}$ = *meso*-tetrakis(*N*-methylpyridinium-4-yl)porphyrin) interact with DNA in a manner similar to the DNA intercalator ethidium bromide as revealed by gel mobility shift assays and viscosity measurements. Both of them also inhibited the topoisomerase I induced relaxation of supercoiled DNA. Complex **4a**, a gold(III) derivative of the known G-quadruplex-interactive porphyrin $[H_2TMPyP]^{4+}$, can similarly inhibit the amplification of a DNA substrate containing G-quadruplex structures in a polymerase chain reaction stop assay. In contrast to these reported complexes, complex **2a** and the parental gold(III)–porphyrin **1a** do not display a significant inhibitory effect ($<10\%$) on telomerase. Based on the results of protein expression analysis and computational docking experiments, the anti-apoptotic bcl-2 protein is a potential target for those gold(III)–porphyrin complexes with apoptosis-inducing properties. Complex **2a** also displays prominent anti-angiogenic properties in vitro. Taken together, the enhanced stabilization of the gold(III) ion and the ease of structural modification render porphyrins an attractive ligand system in the development of physiologically stable gold(III) complexes with anticancer and anti-angiogenic activities.

Keywords: antitumor agents · bioinorganic chemistry · DNA · G quadruplexes · porphyrinoids

Introduction

Although cisplatin and its derivatives remain one of the major classes of chemotherapeutic agents for cancer treatment,[1] their clinical success is compromised by the emergence of drug resistance and toxic side effects.[2] At the same time cisplatin and its derivatives have stimulated considerable interest in metal-based drugs.[3] In the context of developing non-platinum-metal drugs for anticancer treatment, Sadler and co-workers in the early 1980s reported that dimethylgold(III) complexes displayed anticancer activ-

[a] Dr. R. W.-Y. Sun, Dr. C. K.-L. Li, Dr. D.-L. Ma, J. J. Yan, Dr. C.-N. Lok, Dr. C.-H. Leung, Dr. N. Zhu, Prof. Dr. C.-M. Che
Department of Chemistry and Open Laboratory of Chemical Biology of the Institute of Molecular Technology for Drug Discovery and Synthesis, The University of Hong Kong
Pokfulam Road, Hong Kong (China)
Fax: (+852)2857-1586
E-mail: cmche@hku.hk

Supporting information for this article is available on the WWW under http://dx.doi.org/10.1002/chem.200902741.

ity.[4] In recent years, a number of gold(III) complexes were reported to be more effective at inhibiting cancer cells than clinically used cisplatin, with IC_{50} values at the micromolar level.[5] However, most of these cytotoxic gold(III) complexes are susceptible to spontaneous reduction to gold(I) and colloidal gold under physiological conditions.[5,6] In the literature, there are only a few cytotoxic gold(III) complexes, including $[Au^{III}(bipy^{c}\text{-}H)(OH)][PF_6]$ ($bipy^{c}\text{-}H$ = deprotonated 6-(1,1-dimethylbenzyl)-2,2′-bipyridine),[6u] $[Au^{III}(dmamp)Cl_2]$ (dmamp = 2-(dimethylaminomethyl)phenyl),[7] $[Au^{III}{}_m(C\text{^}N\text{^}C)_mL]^{n+}$ (m = 1–3; n = 0–3; HC^N^CH = 2,6-diphenylpyridine),[8] and the $[Au(Por)]^+$ complexes (Por = porphyrinato ligand)[9] that are known to exhibit significant anticancer activity, as well as excellent solution stability.

An understanding of the cytotoxic action of gold(III) complexes is still in its rudimentary stages.[5,6] Historically, gold(III) complexes were proposed to act similarly to cisplatin by executing their anticancer activities through covalent binding to DNA molecules.[5,10] Recently, proteasome[5a] and thioredoxin reductase[5d] have been proposed to be molecular targets of gold(III) complexes. In previous work, we employed a simple porphyrin ligand *meso*-tetraphenylporphyrin (H_2TPP) to stabilize the gold(III) ion, and reported that $[Au^{III}(TPP)]Cl$ (**1a**) exhibits significant in vitro and in vivo anticancer activity through modes of action that are different to those of cisplatin.[5c,9] We also reported that $[Au^{III}(p\text{-}Y\text{-}TPP)]Cl$ (Y = Me, OMe, Br, or Cl) undergo reversible electrochemical reduction at potentials ≤ -0.96 V versus $Cp_2Fe^{+/0}$ (Cp = cyclopentadienyl), revealing that the porphyrin ligand stabilizes the gold(III) ion against demetalation upon reduction in solution.

Gold(III)–porphyrins are planar lipophilic cations. The strategy of using lipophilic cations to target mitochondria in cancer treatment has previously been proposed.[11] Planar aromatic organic cations, such as terephthalanilide, were reported to be cytotoxic,[12] and rhodamine 123 (Rh123) and dequalinium chloride (DECA) are two examples of lipophilic cations that have advanced to extensive in vivo studies.[11,12] Notably, the water-soluble rhodacyanine MKT-077 has been advanced to clinical trials.[13] However, the synthesis as well as structural modification of planar π-conjugated organic cations is a formidable challenge. Berners-Price, McKeage, and co-workers showed that the lipophilic metal cations $[Au^{I}(dppe)_2]^+$ (dppe = 1,2-bis(diphenylphosphino)-ethane) and their derivatives display potent in vitro and in vivo anticancer activities by inducing mitochondrial-mediated apoptotic cell death.[14] Importantly, the biological efficacies of $[Au^{I}(p\cap p)_2]^+$ (p∩p = diphosphine ligand) were found to correlate to their lipophilicity.[14,15] Through coordination of the dianionic porphyrin ligand to gold(III) ion, we have developed a series of $[Au(Por)]^+$ complexes with "tunable" lipophilicity, which allows one to examine the structure–bioactivity relationship.

Results

The structures of the gold(III)–porphyrin complexes are depicted in Scheme 1. These gold(III) complexes, including 16 new derivatives **1f–1i**, **2a–2d**, **3**, and **5a–5g**, are grouped into five categories: I, **1a–1i**; II, **2a–2d**; III, **3**; IV, **4a** and **4b**; and V, **5a–5g**. All of these gold(III)–porphyrin complexes except complex **3**, contain tetraarylporphyrin ligands. The porphyrin ligands employed in this work were prepared according to the method of Adler et al.[16a] The synthesis of glycosylated porphyrins involves the condensation of the pyrrole and *para*-glycosylated benzaldehyde.[16b] With the exception of **4a** and **4b**, metalation of porphyrin ligands with a gold(III) salt was achieved by following a protocol described by Fleischer and Laszlo.[17a] For the synthesis of complexes **4a** and **4b**, a procedure reported by Harriman and co-workers was employed, and both of the complexes were obtained in about 35% yield by using 10% aqueous pyridine as the solvent.[18]

The gold(III)–porphyrin complexes were characterized by UV/Vis and NMR spectroscopies, as well as mass spectrometry. The spectral data are compiled in the Experimental Section. The absorption spectra of the gold(III)–porphyrin complexes are characterized by a reduced number of Q bands and a blue (hypsochromic) shift of the intense Soret band (B band). These spectral features were previously explained by Au^{III}–N bonding interactions, consequently leading to stabilization of the HOMO levels, and an increase in the HOMO–LUMO gap with respect to that of the metal-free porphyrin.[17b] Except for the anionic gold(III) complex **4b**, the positive-ion mass spectra of all the gold(III)–porphyrins display cluster peaks, which are attributed to the parental $[M^+]$ ions. The ^{1}H NMR spectra of the gold(III)–porphyrins (Types I to V) reveal a downfield shift of the pyrrolic protons to approximately $\delta_H = 9$ ppm; attributable to the inductive effect of the gold(III) ion. This inductive effect on the H_m and H_o protons is less significant, since comparable δ_H values were found for both the free and metalated porphyrins.[16c,d]

The ^{1}H NMR spectra and spectral assignments of Type II (**2a–2d**) and Type V (**5a–5g**) complexes are given in the Supporting Information (Figures S1–S11) and the Experimental Section. The OH protons of **2a** and **2c**, and the COOH protons of **5b** and **5c**, are difficult to locate due to their fast exchange reactions in deuterochloroform or deuteromethanol. The pyrrolic and phenyl proton signals of Type II glycosylated gold(III)–porphyrins are similar to those of $[Au(TPP)]^+$. Assignments of the ^{1}H NMR signals were made based on integration and by comparing the chemical shifts with those of the reported metal-free porphyrin ligands.[16c,d] By using **2a** as an example for discussion, there are three sets of signals centered at $\delta = 9.39$, 8.18, and 7.63 ppm corresponding to H_β, H_o, and H_m, respectively. These signals are shifted downfield compared with that of the metal-free 5,10,15,20-tetrakis(4-β-D-glucosylphenyl)porphyrin ($\delta = 9.13$, 8.09, and 7.52 ppm for H_β, H_o, and H_m, respectively). In contrast, the shifts of the protons of the gly-

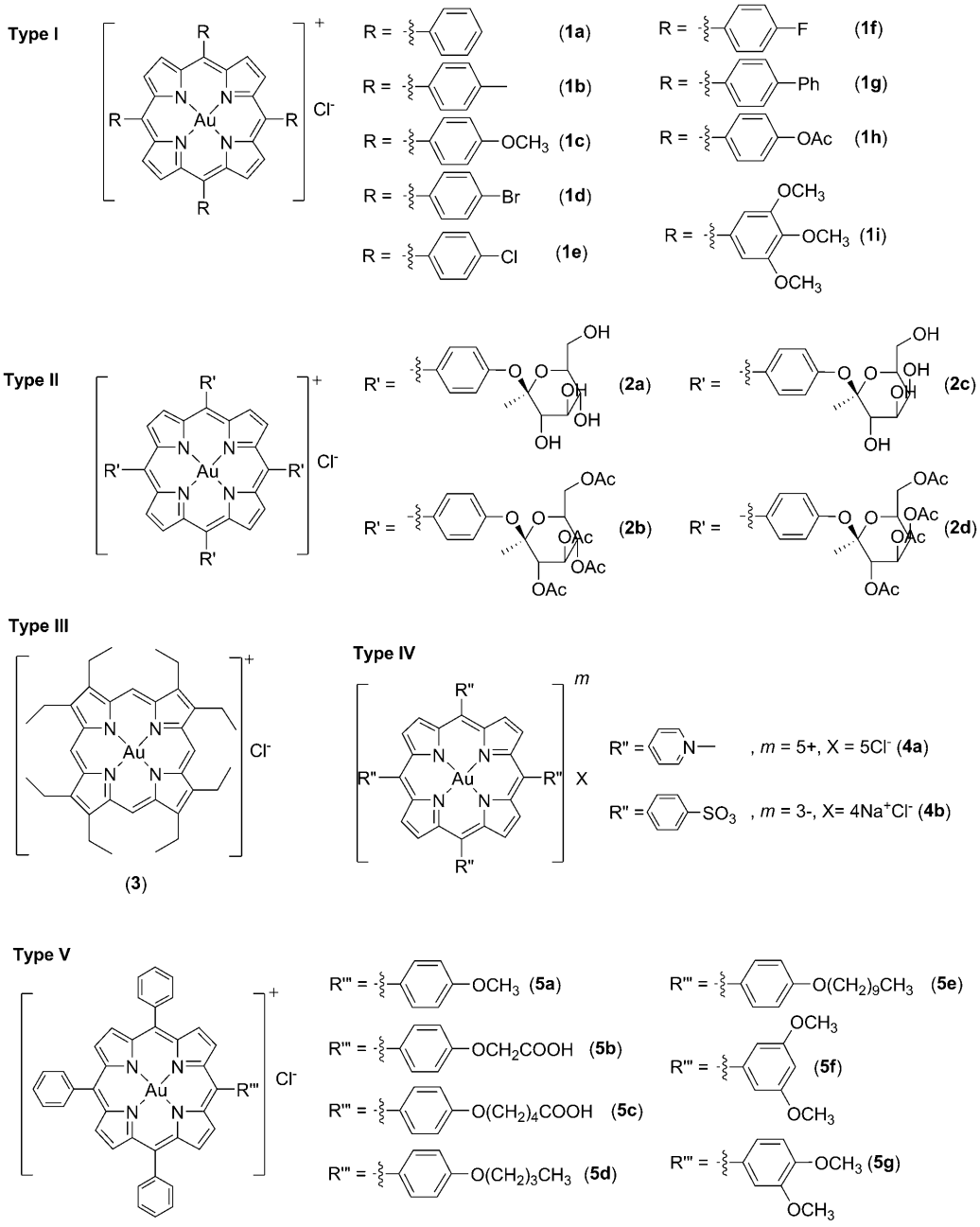

Scheme 1. The gold(III)–porphyrin complexes.

cosylated moieties in **2a** are similar to those of the reported *ortho*-glycosylated porphyrins (between $\delta = 3.4$ and 4.2 ppm).[16d]

X-ray crystal structures: The structures of $[Au^{III}(TPP)](ClO_4)$ (Figure S12 in the Supporting Information),[9i] $[Au^{III}(p\text{-F-TPP})](Au^{I}Cl_2)$ (Figure S13 in the Supporting Information), and **1g** (Figure S14 in the Supporting Information) were determined by X-ray crystallography. The crystallographic data-collection parameters and selected bond angles and distances for $[Au^{III}(p\text{-F-TPP})](Au^{I}Cl_2)$ and **1g** are given in the Supporting Information (Tables S1 and S2, respectively). All of the structures reveal a square-planar geometry, with almost four identical N-Au-N angles (N-Au-N, $[Au^{III}(TPP)](ClO_4)$: 89.8–90.1°; $[Au^{III}(p\text{-F-TPP})](Au^{I}Cl_2)$: 88.1–91.9°; and **1g**: 89.8–90.2°) and Au–N(pyrrolic) distances (Au–N, $[Au^{III}(TPP)](ClO_4)$: 2.032–2.033 Å; $[Au^{III}(p\text{-F-TPP})](Au^{I}Cl_2)$: 2.010–2.015 Å; and **1g**: 2.001–2.015 Å). There is no close contact between the counteranion and $[Au(Por)]^+$ cation in the crystal structures.

Solubility and stability: All of the gold(III) complexes are soluble in DMSO, with a solubility of $>10\,mg\,mL^{-1}$ (except **1g**, its solubility is $\approx 0.1\,mg\,mL^{-1}$ in DMSO). Complexes

with hydroxy (**2a** and **2c**) or carboxy (**5b** and **5c**) substituents at the periphery of the porphyrin ligand have an aqueous solubility of $\approx 0.5\ mg\,mL^{-1}$; complexes **4a** and **4b**, with charged substituents at the periphery have an aqueous solubility of at least $10\ mg\,mL^{-1}$. All of the gold(III)–porphyrins except **1g** are soluble in phosphate-buffered saline (PBS, 50 mM phosphate, 4 mM NaCl, pH 7.4 at 25 °C) containing 5% DMSO at 0.1 mM level. No significant UV/Vis spectral changes for any of the complexes were observed over 72 h at room temperature, and no demetalation was observed in any case.

In vitro cytotoxicity: By means of 3-(4,5-dimethylthiazol-2-yl)-2,5-diphenyltetrazolium bromide (MTT) assays,[19] the in vitro cytotoxicity of the gold(III)–porphyrin complexes was evaluated by using human nasopharyngeal carcinoma (NPC) cell lines (SUNE1, HK1, and HONE1), a human melanoma cell line (UACC-903), and a normal human lung fibroblast-derived cell line (CCD-19Lu). Figure 1a depicts the percentage cell survival of the SUNE1 cells versus the concentrations of **1a**, **2a**, **3**, **4a**, and **5a** for an incubation period of 72 h, with cisplatin for comparison. From the cytotoxicity profiles, the IC_{50} values of **1a**, **2a**, **3**, **4a**, **5a**, and cisplatin were determined to be 0.056, 1.8, 0.84, 82, 0.091, and 8.5 μM, respectively. The IC_{50} values of the other gold(III)–porphyrin complexes were similarly evaluated. As depicted in Table 1, the complexes of Types I (**1a**–**1f** and **1h**), III (**3**), and V (**5a** and **5c**–**5g**) exhibit potent cytotoxicity toward the cancer cell lines, with IC_{50} values ranging from 0.033 to 6.8 μM. Notably, complex **1a** (IC_{50}: 0.033 to 0.14 μM) is highly active against all the cancer cell lines, and is 61 (HONE1) to 152 (SUNE1) times more potent than cisplatin under the same conditions.

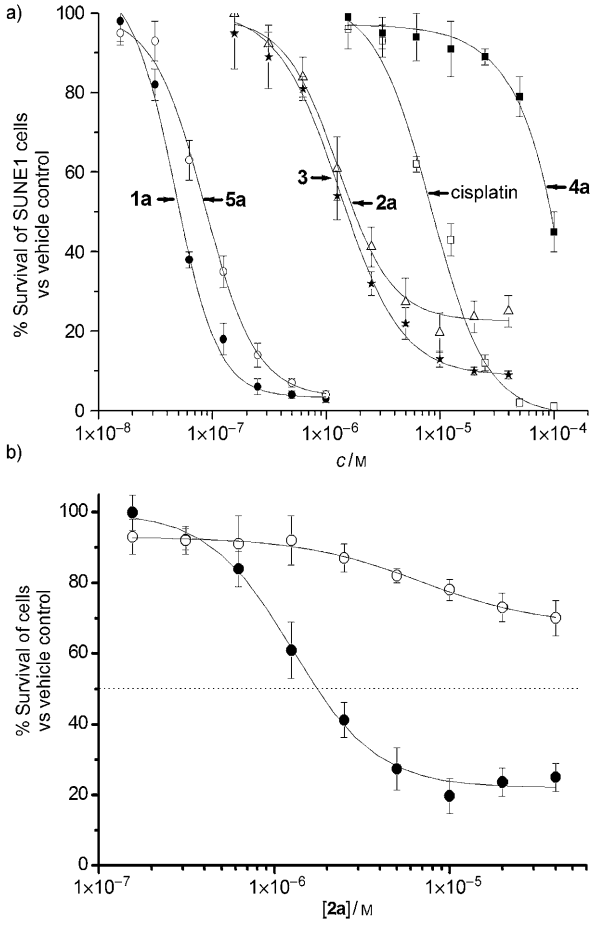

Figure 1. a) Drug-sensitivity profiles of SUNE1 cells treated with **1a**, **2a**, **3**, **4a**, **5a**, and cisplatin for 72 h. b) Drug-sensitivity profiles of **2a** toward normal lung fibroblast CCD-19Lu (○) and nasopharyngeal SUNE1 cells (●). Graph shows the percentage cell death versus vehicle control upon incubation of increasing concentrations of **2a**.

Type II complexes contain saccharide-conjugated porphyrinato ligands. Although complexes **2a**–**2d** are less potent than the parental complex **1a**, complex **2a** was found to exhibit cytostatic inhibition of proliferation instead of cytotoxic (cell-killing) activity. According to the cell proliferation profiles (formazan absorbance $A_{550\,nm}$ versus incubation time, Figure S15 in the Supporting Information), SUNE1 cells treated with 0.1 to 10 times the IC_{50} concentration of **2a** (0.18, 1.8, and 18 μM) had a constant viable cell number during the period of drug treatment (72 h). No significant cell death (<10%) was detected by the trypan blue exclusion assay. Thus, only the cellular proliferation was inhibited by treatment with **2a**. The metal-free, saccharide-conjugated porphyrin of H_2(4-glucosyl-TPP) (*meso*-tetrakis(4-β-D-glucosylphenyl)porphyrin) also showed cytostatic activity toward SUNE1 cells with an IC_{50} value of 7.7 μM, albeit being approximately 4.3-fold lower in inhibitory activity than that of **2a**.

[Au^{III}(OEP)]Cl (**3**, Type III) is also highly cytotoxic (IC_{50}: 0.078–0.84 μM) to all the cancer cell lines examined in this work. Complexes **4a** and **4b** (Type IV), both having multiple charges at the periphery of the porphyrin ligand, are relatively less toxic, with IC_{50} values >50 μM toward all of the cancer cell lines examined. The methoxy substituents at the peripheral phenyl ring of complexes **5a**, **5f**, and **5g** do not have a significant effect on the cytotoxicity in any of the cancer cell lines examined. Complexes **5b**–**5e**, which have peripheral $-OCH_2COOH$, $-O(CH_2)_4COOH$, $-O(CH_2)_3CH_3$, and $-O(CH_2)_9CH_3$ substituents on one of the *meso*-phenyl rings, respectively, are at least 10-fold less cytotoxic than **1a**.

Most of the gold(III)–porphyrin complexes examined in this work exhibited higher selective cytotoxicity to nasopharyngeal cancer cells than to normal lung fibroblast-derived cells (CCD-19Lu cell line). For example, both **1a** (Type I) and **5a** (Type V) are cytotoxic and exhibited 5.8- and 3.2-fold higher cytotoxicity, respectively, toward the cancer cell lines than to noncancerous cells (HONE1 vs. CCD-19Lu). Although Type II complexes (**2a**–**2d**) are not cytotoxic, they display cytostatic activities preferentially toward cancer cell lines. For example, complex **2a** is cytostatic to NPC cells (SUNE1, HK1, and HONE1) with IC_{50} values ranging from 1.2 to 3.6 μM, whereas it is relatively nontoxic to CCD-19Lu fibroblast cells with the IC_{50} value determined to be more than 100 μM (Figure 1b), revealing at least 28-fold selectivity

Table 1. In vitro cytotoxicity of the gold(III)–porphyrin complexes toward selected cancer and normal cell lines.

Complex	IC_{50} [μM] SUNE1[a]	HK1[a]	HONE1[a]	UACC-903[a]	CCD-19Lu[a]
1a	0.056±0.007	0.081±0.015	0.033±0.004	0.14±0.03	0.19±0.02
1b	0.31±0.02	6.8±0.4	0.10±0.02	1.5±0.2	0.45±0.03
1c	0.30±0.05	0.24±0.07	0.085±0.013	0.67±0.12	0.18±0.05
1d	1.5±0.2	0.3±0.04	0.43±0.02	1.5±0.2	0.89±0.13
1e	0.66±0.12	3.5±0.7	0.55±0.11	1.9±0.2	0.56±0.12
1f	0.21±0.03	0.23±0.11	0.14±0.01	0.31±0.08	0.22±0.08
1g	12±2	14±3	23±2	34±5	>100
1h	0.21±0.05	0.17±0.02	0.099±0.012	0.17±0.04	1.1±0.5
2a	1.8±0.4	3.6±1.1	1.2±0.2	9.0±1.2	>100
2b	9.1±1.4	2.5±0.4	11±1	9.8±2.6	>100
2c	2.6±0.5	3.0±0.9	6.5±1.4	11±3	>100
2d	10±3	2.3±0.2	12±2	14±1	>100
3	0.84±0.11	0.11±0.07	0.078±0.006	0.38±0.07	0.97±0.13
4a	82±7	>100	63±2	52±4	>100
4b	50±4	>100	80±3	>100	>100
5a	0.091±0.021	0.13±0.04	0.053±0.007	0.29±0.09	0.17±0.03
5b	3.6±0.3	13±2	2.7±0.4	3.5±0.3	5.9±1.2
5c	0.88±0.09	0.64±0.09	0.45±0.06	0.84±0.14	1.0±0.1
5d	2.7±0.3	0.97±0.14	0.98±0.17	n.d.[b]	3.2±0.5
5e	0.62±0.13	0.52±0.07	0.38±0.04	n.d.[b]	0.98±0.17
5f	0.21±0.06	0.14±0.03	0.062±0.012	0.16±0.03	0.17±0.05
5g	0.19±0.04	0.36±0.02	0.049±0.014	0.15±0.04	0.099±0.017
cisplatin	8.5±1.1	5.9±0.7	2.0±0.7	21±3.8	>100

[a] SUNE1, HK1, and HONE1 = human nasopharyngeal carcinoma cell lines; UACC-903 = human melanoma cell line; CCD-19Lu = human normal lung fibroblast cells. [b] n.d. = not determined.

toward various NPC cell lines over noncancerous fibroblast cells.

Relationship between in vitro anticancer activities and lipophilicity: Previous reports revealed that the biological activities of porphyrins and metalloporphyrins were affected by their overall lipophilicity.[20] In this work, the relationship between the lipophilicity of the gold(III)–porphyrin complexes and their in vitro anticancer activities was examined. Their lipophilicity was measured by means of *n*-octanol/water partitioning by using a flask-shaking method.[21] The lipophilicity parameter ($\log P$) is defined as the logarithmic ratio of the drug concentration in the organic phase (*n*-octanol) to that in the aqueous phase (Table 2). The gold(III)–porphyrin complexes have $\log P$ values ranging from −1.85 to 1.95. The correlation between lipophilicity and cytotoxicity toward SUNE1 cells for the gold(III)–porphyrin complexes is depicted in Figure 2. The complexes with positive $\log P$ values are more cytotoxic. The two glycosylated gold(III) complexes (Type II, **2a** and **2c**) with the least positive $\log P$ values were cytostatic. Type IV gold(III)–porphyrin complexes, which have charged substituents at the porphyrin ligand periphery have the most negative $\log P$ values and weak cytotoxicity.

Relationship between in vitro anticancer activities and cellular uptake: Lipophilicity determines the efficiency of cellular uptake, and hence, the overall biological activity of a compound or metal complex.[21,22] To examine the relationship between cellular uptake and the cytotoxicity of the gold(III)–porphyrin complexes, the gold content of the cells treated with the complexes for 4 h was measured by means of inductively coupled plasma mass spectrometry (Table 2). As depicted in Figure 3, the cellular uptake of the gold(III) complexes displays a logarithmic dependence on the lipophilicity.

Hemolysis: Charged lipophilic compounds have been reported to strongly bind to the cell membrane, with the result that membrane toxicity is also of great concern.[21] In this work, we assayed the membrane toxicity of the gold(III)–porphyrin complexes by using an erythrocyte (red blood cell) hemolysis model. Sodium dodecyl sulfate (SDS, 10 μM), an anionic surfactant used as a positive control, induced over 86.3% hemolysis. As shown in Table 2, all of the gold(III)–porphyrin complexes applied at 0.5 μM induced less than 10% hemolysis. Several cytotoxic gold(III)–porphyrin complexes including **1a** and **5a**, displayed a significant membrane toxicity (>50% hemolysis) at a concentra-

Table 2. Selected physical parameters of the gold(III)–porphyrin complexes.

Complex	Lipophilicity ($\log P$)	Cellular uptake [pg/cell]	Hemolysis at 24 h [%] 0.5 μM	5 μM
1a	1.88	0.056	7.4	97
1b	1.94	0.026	7.4	54
1c	1.70	0.082	3.7	12
1d	1.05	0.0055	4.8	24
1e	1.24	0.0068	4.4	23
1f	1.05	0.054	3.3	30
1g	1.95	0.0014	0.2	2.6
1h	0.92	0.015	8.9	57
2a	0.47	0.0033	2.4	4.3
2b	1.15	0.0169	0.3	2.6
2c	0.55	0.0039	2.2	2.8
2d	1.14	0.0121	0.4	4.9
3	1.81	0.0566	2.6	18.3
4a	−1.85	0.0014	4.1	3.9
4b	−1.43	0.0012	3.1	7.9
5a	1.32	0.0478	1.7	60
5b	0.76	0.0076	4.6	39
5c	0.95	0.035	5.5	32
5d	0.76	0.0079	5.7	68
5e	0.84	n.d.[a]	2.7	7.6
5f	1.76	0.080	8.4	81
5g	1.88	0.063	8.1	86

[a] n.d. = not determined.

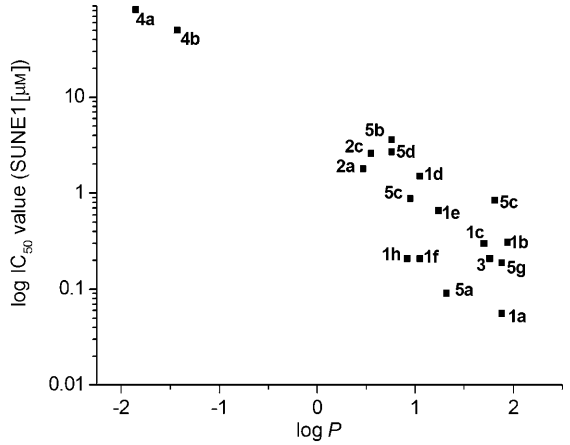

Figure 2. The relationship between cytotoxicity toward SUNE1 cells and lipophilicity of the gold(III)–porphyrin complexes.

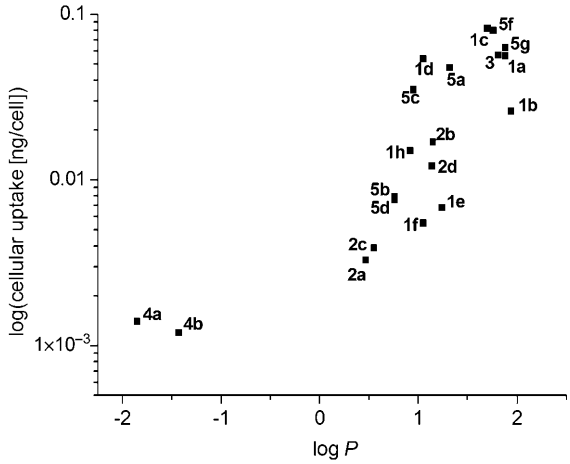

Figure 3. The relationship between gold uptake by SUNE1 cells and lipophilicity of gold(III)–porphyrin complexes.

tion of 5 μM. In contrast, the Type II complexes displayed less than 5% hemolysis in every case.

Flow-cytometric analysis: In this study, cell-cycle analysis was performed to examine whether the gold(III)–porphyrin complexes would affect DNA synthesis,[23] and/or induce apoptosis in cancer cells. We employed fluorescence-activated cell-sorting (FACS) analysis to assess the DNA content of cells stained with propidium iodide (PI). FACS analysis enables quantification of the total cellular population in different phases of the cell cycle (G_1, S, and G_2-M), as well as the sub-G_1 apoptotic population (A). The flow-cytometric diagrams and data for SUNE1 cells treated with **1a**, **2a**, **3**, **4a**, and **5a** at their corresponding IC_{50} concentrations are depicted in Figure 4 and Table 3, respectively. Treatment of cells with the IC_{50} value of **1a** for 24 h increased the percentage of cells in the S phase from 28.2 to 45.2%, in association with decreased percentages of cells in the G_1 and G_2-M phases. Prolonged incubation of **1a** for 48 h further enhanced the S-phase cell-cycle arrest, decreased the portions of cells at the G_1 and G_2-M phases, and increased the percentage of apoptotic cells (A, 26.4%), which were detected as the sub-G_1 population. In addition to **1a**, the cytotoxic complexes **3** and **5a**, and cytostatic complex **2a** also en-

Table 3. Fluorescence-activated cell-sorting analysis showing the percentage of G_1, S, and G_2-M phases of the cell cycle among the live cells, and the percentage of apoptotic cells (A) among the total cells.

Complex	Treatment time [h]	G_1 [%]	S [%]	G_2-M [%]	A [%]
DMSO	24	68.4	28.2	3.4	5.1
	48	55.8	27.1	17.1	13
cisplatin (8.5 μM)	24	65.6	29.9	4.5	4.9
	48	35.9	43.4	20.7	18.2
1a (0.056 μM)	24	47.7	45.2	7.1	15.8
	48	47.5	46.0	6.5	26.4
2a (1.8 μM)	24	53.9	38.3	7.8	3.3
	48	55.4	34.5	10.1	10.2
3 (0.84 μM)	24	66.0	29.4	4.6	4.5
	48	54.9	34.1	11.0	39.7
4a (82 μM)	24	67.1	31.0	4.9	2.5
	48	59.1	28.0	9.9	6.6
5a (0.091 μM)	24	62.4	31.7	5.9	10.6
	48	57.7	36.7	5.6	40.8

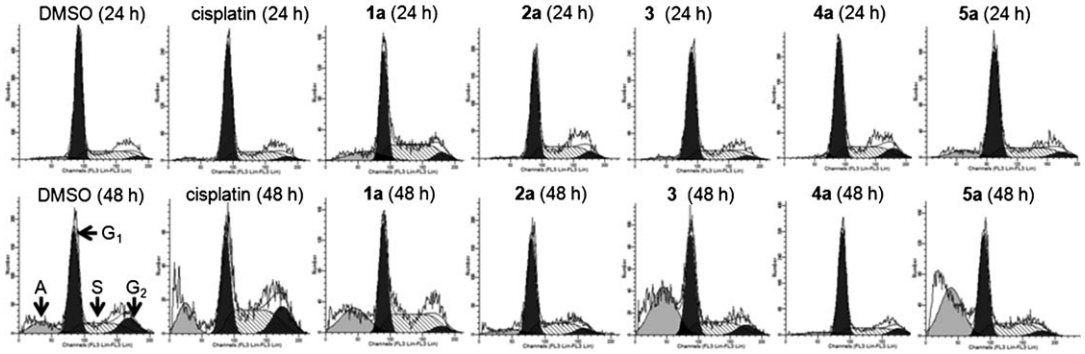

Figure 4. Induction of apoptosis and the cell-cycle arrest in the SUNE1 cancer cells after treatment with gold(III)–porphyrin complexes. SUNE1 cells treated with DMSO (0.5%, v/v), cisplatin (8.5 μM), **1a** (0.056 μM), **2a** (1.8 μM), **3** (0.072 μM), **4a** (82 μM), or **5a** (0.091 μM) were collected after 24 or 48 h of incubation and subjected to flow-cytometric analysis. G_1 = G_1-phase cells; G_2 = G_2-M-phase cells; S = S-phase cells; A = apoptotic cells with subG_1 DNA content.

hanced accumulation of cells in the S phase. Significant percentages of apoptotic cells, that is, 39.7 and 40.8%, were detected upon a 48 h treatment of cells with **3** and **5a**, respectively. In contrast, no apparent increase in apoptotic cell death was detected for cells treated with the cytostatic **2a** or the relatively nontoxic **4a**.

Apoptosis: Apoptosis is a regulated physiological process leading to cell death. Unlike necrosis, apoptosis does not trigger any inflammatory reaction in the tissues. Thus, it is advantageous for chemotherapeutic agents to induce apoptosis in cancer cells. As indicated in the previous section, flow cytometric analysis showed that the cytotoxic complexes **1a** (0.056 μM), **3** (0.84 μM), and **5a** (0.091 μM) induced apoptosis in SUNE1 cancer cells. A family of cysteine–aspartic acid proteases known as caspases are among the central effectors of apoptosis.[24] By using an established enzyme-linked immunosorbent assay (ELISA), we have examined the induced apoptosis, along with the caspase-3 activation, after the gold(III)–porphyrin treatment. We found that complexes **1a**, **3**, and **5a** enhanced caspase-3 activation after a 15 h treatment (Figure S16, in the Supporting Information). Neither the cytostatic complex **2a** (1.8 μM) nor the relatively nontoxic complex **4a** (82 μM) induced cancer cell death or caspase-3 activation.

Interactions with DNA: As mentioned in the previous section, the gold(III)–porphyrin complexes triggered S-phase cell-cycle arrest in cancer cells. This is indicative of a halt in DNA synthesis. We thus examined the DNA binding activity of **1a** (Figure S17 in the Supporting Information), **2a** (Figure 5), **3** (Figure S18 in the Supporting Information), **4a** (Figure S19 in the Supporting Information), and **5a** (Figure S20 in the Supporting Information) by means of UV/Vis absorption titration experiments.[25] By using **2a** as an example, isosbestic spectral changes at 310, 421, and 527 nm, and hyperchromicity (47.2%, Table 4) of the Soret band

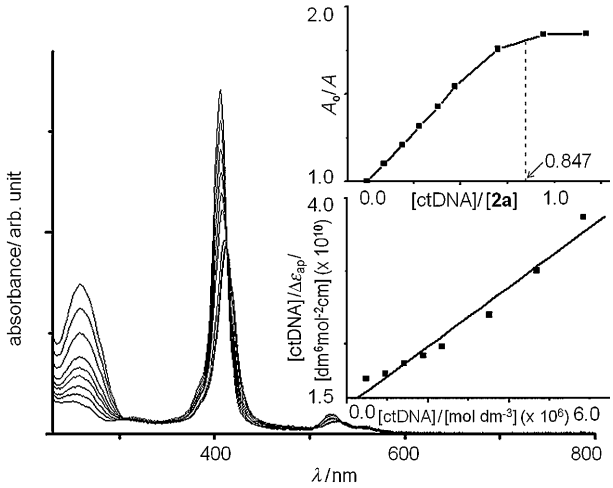

Figure 5. UV/Vis spectral changes of **2a** in TBS/DMSO (9:1) with increasing concentration of ctDNA at 292.8 K. Inset: plots of A_o/A versus [ctDNA]/**2a** and [ctDNA]/$\Delta\varepsilon_{ap}$ versus [ctDNA]. Absorbance was monitored at 410 nm.

Table 4. DNA binding parameters for selected classes of gold(III)–porphyrin complexes at 298 K.

Complex	Binding constant (K_b) [dm^3mol^{-1}]	Hypochromicity [%]
1a	$(2.8\pm0.2)\times10^6$	53.4
2a	$(5.8\pm0.3)\times10^5$	47.2
3	$(4.1\pm0.2)\times10^6$	30.1
4a	$(4.9\pm0.4)\times10^5$	47.8
5a	$(1.9\pm0.2)\times10^6$	28.9

(405 nm), were observed upon addition of calf thymus DNA (ctDNA, 0–5 μM) to a solution of **2a** in Tris-buffered saline containing 5% DMSO.

The binding constant (K_b) for **2a** toward ctDNA was obtained from the plot of [ctDNA]/$\Delta\varepsilon_{ap}$ against [ctDNA] according to the Scatchard equation [Eq. (1)]:

$$[\text{ctDNA}]/\Delta\varepsilon_{ap} = [\text{ctDNA}]/\Delta\varepsilon + 1/(\Delta\varepsilon \times K_b) \quad (1)$$

in which $\Delta\varepsilon_{ap} = |\varepsilon_A - \varepsilon_B|$, $\varepsilon_A = A_{obs}/[\text{complex}]$, and $\Delta\varepsilon = |\varepsilon_B - \varepsilon_F|$. The symbols ε_B and ε_F correspond to the extinction coefficient of DNA-bound and unbound **2a**, respectively. By using the absorbance data of **2a**, the plot of [ctDNA]/$\Delta\varepsilon_{ap}$ versus [ctDNA] gives a straight line ($R=0.98$) with a slope of 2.7×10^{-4}, which corresponds to the reciprocal of the $\Delta\varepsilon$ value (inset of Figure 5). From the intercept of the plot, the binding constant for **2a** to ctDNA was determined to be $(5.8\pm0.3)\times10^5\ dm^3mol^{-1}$ at 298 K. Similar absorption titration experiments with **1a**, **3**, **4a**, and **5a** were performed (Figures S17–S20 in the Supporting Information), and the corresponding binding constants to ctDNA are summarized in Table 4. The binding constants of all of the five gold(III)–porphyrin complexes toward ctDNA are similar, being in the range from 4.9×10^5 to $4.1\times10^6\ dm^3mol^{-1}$.

DNA intercalators, such as ethidium bromide (EB), are known to cause DNA elongation.[26] Thus, EB-intercalated DNA would have a lower electrophoretic mobility and a higher viscosity than that of free DNA. In this work, a gel mobility shift assay and viscosity measurements were performed to examine whether the gold(III)–porphyrin complexes would function as a DNA intercalator. DNA ladders (100 base pairs) alone and those treated with the gold(III)–porphyrin complexes or EB (1 μM) were mixed and resolved by agarose gel electrophoresis. As depicted in Figure 6, the DNA samples treated with **1a**, **3**, and **5a** displayed similar mobility as that of the untreated DNA ladder. In contrast, the DNA samples treated with **2a**, **4a**, or EB showed retarded mobility (tailing effect), which may be attributed to intercalation into the DNA base pairs. By viscosity measurements, we confirmed that only **2a**, **4a**, and EB increased the viscosity of the DNA solution (Figure S21 in the Supporting Information). These results further suggest that **2a** and **4a** (but not **1a**, **3**, or **5a**) bind to DNA through intercalation.

Hurley and co-workers reported that free porphyrins, and certain metallo-derivatives of which, inhibit the activity of DNA enzymes, such as telomerase, and cause downregulation of c-*myc* transcription through G-quadruplex stabiliza-

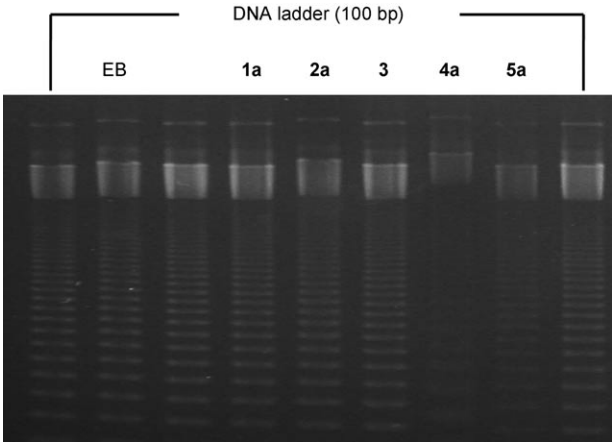

Figure 6. Gel electrophoresis of 100 bp DNA ladder (15.2 μM in base pairs) in 2% (w/v) agarose gel showing the mobility of the DNA in the absence (first and last lanes) or the presence of ethidium bromide (EB), Hoechst33342 (H), **1a**, **2a**, **3**, **4a**, or **5a** in a 1:1 ratio of DNA base pairs to the complex.

tion.[27] In this study, we examined the effects of gold(III)–porphyrin complexes on the stabilization of G-quadruplex DNA by means of a polymerase chain reaction (PCR) stop assay.[28] This assay includes the use of a G-quadruplex forming oligomer Pu27 (5′-TGGGGAGGGTGGGGAGGGTGGGGAAGG-3′) and its partially overlapping complementary sequence. In the absence of the G-quadruplex forming agent, the *Taq* polymerase present in the reaction mixture amplifies Pu27, leading to the formation of a double-stranded PCR product, which can be resolved by polyacrylamide gel electrophoresis (PAGE). In contrast, the G-quadruplex stabilizing agent facilitates the formation of the G-quadruplex of the Pu27 oligomer and subsequently halts the DNA amplification. As shown in Figure 7, the cytotoxic complexes **1a**, **3**, and **5a**, and the cytostatic complex **2a**, did not impede the PCR with Pu27, revealing that these complexes do not favor the formation of the G-quadruplex. In contrast, complex **4a**, a gold(III) derivative of $[H_2TMPyP]^{4+}$ $[H_2TMPyP]^{4+}$ = *meso*-tetrakis(*N*-methylpyridinium-4-yl)porphyrin), inhibited the PCR amplification, presumably by stabilizing the G-quadruplex structure.

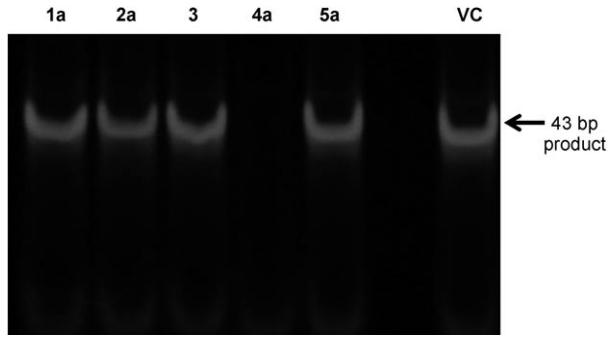

Figure 7. PCR stop assay by using G-quadruplex-forming Pu27 oligomers in the presence of gold(III)–porphyrin complexes with doses corresponding to their cytotoxic IC_{50} values to SUNE1 cells; **1a** (0.056 μM), **2a** (1.8 μM), **3** (0.84 μM), **4a** (82 μM), and **5a** (0.091 μM). The arrow indicates the 43 bp PCR product. VC = vehicle control.

In addition to the effect of the gold(III)–porphyrin complexes on G-quadruplex formation, we also examined the effect on telomerase activity by using the commercially available TeloTAGGG Telomerase PCR ELISA approach. Upon incubation with the telomerase at 37 °C for 10 min, complexes **1a** (7.4% inhibition), **2a** (3.2% inhibition), **3** (5.3% inhibition), and **5a** (6.9% inhibition) all displayed weak inhibition of telomerase addition of telomeric repeats (TTAGGG) to the 3′ end of the biotin-labeled synthetic primer versus vehicle control. In contrast, the reported telomerase inhibitors **4a** and $[H_2TMPyP]^{4+}$ significantly inhibited telomerase, with 57 and 85% inhibition, respectively.

We further examined whether the anticancer mechanism of the cytotoxic gold(III)–porphyrin complexes may involve inhibition of DNA topoisomerase, which catalyzes topological changes in DNA by the formation of transient DNA strand breaks, and are molecular targets of several DNA-binding anticancer drugs.[29] As shown in Figure 8, DNA topoisomerase I (Topo I) induced the formation of the nicked or relaxed supercoiled form of the tertiary DNA structure, which could be inhibited by camptothecin (CPT), a Topo I inhibitor. In the presence of complex **2a** or **4a**, the Topo I catalyzed DNA relaxation was also inhibited. In contrast, complexes **1a**, **3**, and **5a** did not inhibit the Topo I reaction. The ability of the gold(III)–porphyrin complexes to affect the topoisomerase reaction may be related to their modes of DNA binding as intercalators.

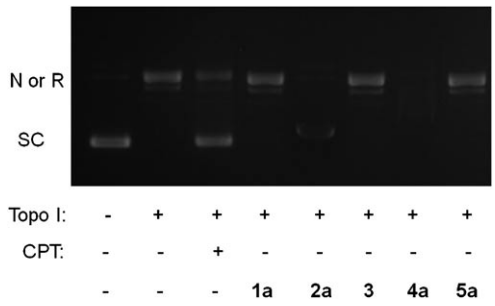

Figure 8. DNA Topo I-induced plasmid DNA relaxation and the effects of **1a** (0.056 μM), **2a** (1.8 μM), **3** (0.072 μM), **4a** (82 μM), **5a** (0.091 μM), or CPT (50 μM). N or R = nicked or relaxed DNA; SC = supercoiled DNA.

Interaction with protein targets: Previously, we demonstrated that the bcl-2 family of proteins are modulated by the anticancer gold(III) complexes.[9] In this work, Western blotting experiments revealed that the expression level of bcl-2, an anti-apoptotic protein residing in the outer membrane of mitochondria, was suppressed after a 15 h treatment of SUNE1 cells with **1a** (Figure 9a), whereas the expression level of another anti-apoptotic protein of the bcl-2 family, mcl-1, was unaltered (Figure S22, in the Supporting Information). The bcl-2 expression of SUNE1 cells treated with **2a** (1.8 μM), **3** (0.84 μM), **4a** (82 μM), and **5a** (0.091 μM) at

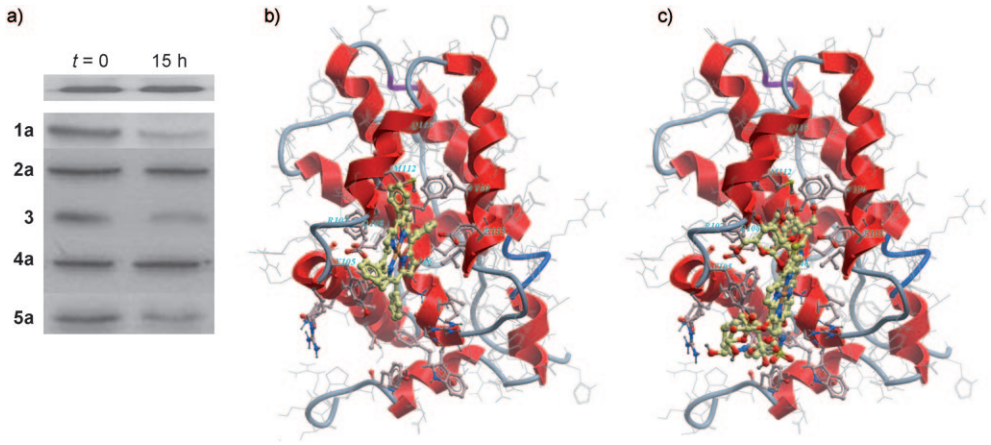

Figure 9. a) The expressions of the bcl-2 protein in gold porphyrin treated SUNE1 cells as revealed by a Western blotting experiment. Molecular docking studies of the bcl-2 protein (PDB code: 2O21) with b) **1a**, and c) **2a**.

doses corresponding to their IC_{50} values for 0 and 15 h are depicted in Figure 9a. Similar to **1a**, cytotoxic complexes **3** and **5a** also downregulated the bcl-2 expression.

In addition, we examined whether the direct binding of **1a** to bcl-2 is a crucial event for the **1a**-induced apoptosis. By computational molecular docking (Internal Coordinate Mechanics (ICM) approach), the energy of binding between **1a** and bcl-2 (protein data bank ID = 2O21) was computed. As depicted in Figure 9b, complex **1a** exhibits a high binding affinity toward bcl-2, and is positioned in a cleft adjacent to amino acid residues Y105, R107, D108, M112, Q115, V130, E133, and A146 with a calculated binding energy of $-20.0\ kcal\,mol^{-1}$. For comparison, the reported bcl-2 inhibitor, an acylsulfonamide-based ligand,[30] has a similar calculated binding energy of $-23.0\ kcal\,mol^{-1}$ toward the bcl-2 protein. In contrast, complex **1a** shows a low binding affinity toward mcl-1 with a calculated binding energy of $-4.78\ kcal\,mol^{-1}$ (Figure S23 in the Supporting Information). Complexes **3** (Figure S24, in the Supporting Information) and **5a** (Figure S26, in the Supporting Information) also have a favorable binding affinity toward bcl-2, with binding energies of -15.9 and $-21.6\ kcal\,mol^{-1}$, respectively (Table 5). In contrast, the cytostatic complex **2a** (Figure 9c) and the relatively nontoxic complex **4a** (Figure S25, in the Supporting Information) both have low binding affinities (**2a**: $+14.5\ kcal\,mol^{-1}$, **4a**: $-10.7\ kcal\,mol^{-1}$) toward this protein.

Thioredoxin (Trx) and thioredoxin reductase (TrxR) systems maintain the cellular redox status by regulating thiol–disulfide exchange. Inhibition of TrxR has recently been shown to be a crucial event for several cytotoxic non-porphyrin-type gold(III) complexes and other transition-metal complexes.[5d,31] In this study, we assessed the ability of the gold(III)–porphyrin complexes to inhibit TrxR by using dithionitrobenzoic acid (DTNB) as the substrate. At concentrations corresponding to the respective growth inhibition, complexes **1a**, **2a**, and **3** were found to exhibit over 60% inhibition of TrxR compared with the vehicle control (Figure S27 in the Supporting Information), whereas **4a** and **5a** displayed relatively lower inhibitory activities (30 and 18%, respectively).

Table 5. Energies of binding between bcl-2 protein and gold(III)–porphyrin complexes as determined by computational molecular docking.

Complex	Binding energy [$kcal\,mol^{-1}$]
1a	−20.0
2a	+14.5
3	−15.9
4a	−10.7
5a	−21.6

In vitro anti angiogenesis: Recently, a benzothiazole-substituted quinol compound has been found to be a potent Trx/TrxR inhibitor and at the same time to display favorable anti-angiogenic activity in vitro.[32] Our previous microarray experiments revealed that **1a** downregulated the genes that play major roles in angiogenesis.[9e] In this study, we examined the cytostatic complex **2a**, cytotoxic complex **3**, and the relatively nontoxic complex **4a** for their anti-angiogenic properties. Since endothelial cell proliferation is one of the initial steps in the angiogenesis, we employed a tube formation assay to measure the formation of capillary-like networks of the endothelial cells. This assay was performed by seeding endothelial MS1 cells on a Matrigel layer. As depicted in Figure 10, treatment of MS1 cells with **2a** and **3** for 8 h drastically reduced endothelial cord formation on the Matrigel compared with the vehicle control. In contrast, no significant inhibition of endothelial cord formation was found for the cells treated with **4a**. A parallel MTT assay was performed for all of the gold(III)–porphyrin complexes at the tested concentrations, and over 90% of the cells remained viable after an 8 h incubation with these gold complexes. The metal-free porphyrins, including H_2(4-glucosyl-TPP) and $[H_2TMPyP]^{4+}$, have an adequate solubility in aqueous medium for biological experiments and their in vitro anti-angiogenic activity has also been evaluated. We found that H_2(4-glucosyl-TPP) has a significant anti-angiogenic activity when applied at 1.8 μM to MS1 cells, revealing

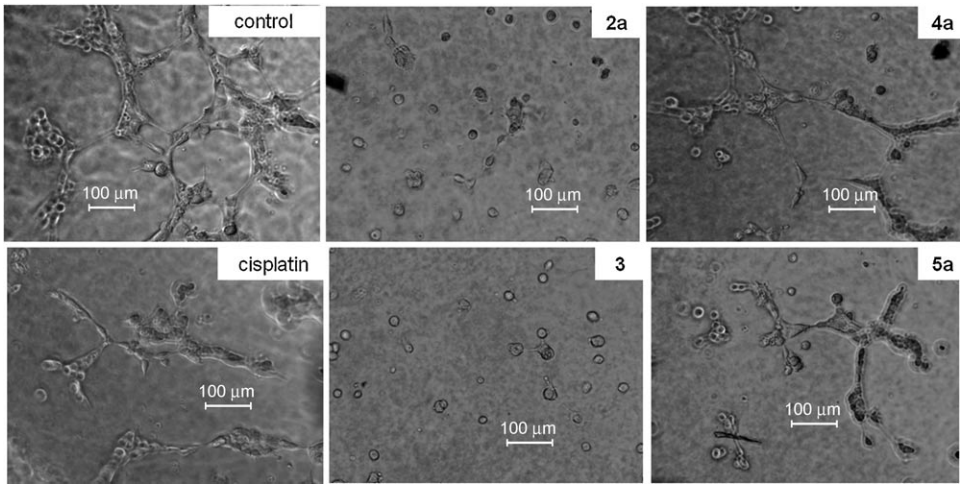

Figure 10. Images of angiogenesis examined by a tube formation assay. MS1 cells were treated with cisplatin (8.5 μM), **2a** (1.8 μM), **3** (0.84 μM), **4a** (82 μM), or **5a** (0.091 μM) and incubated for 8 h.

that the saccharide conjugation may play a role in the anti-angiogenic activity. On the other hand, $[H_2TMPyP]^{4+}$ is neither cytotoxic nor anti-angiogenic.

Synergistic effects of the co-treatment of gold porphyrin complexes with an organic dye: Apart from the aforementioned cytotoxic, cytostatic, and anti-angiogenic activities, the gold(III)–porphyrin complexes also demonstrated a synergistic effect upon incubation with the fluorescent dye 4′,6-diamidino-2-phenylindole (DAPI). DAPI has a strong binding affinity to DNA and fluoresces upon binding, but it is not readily cell permeable. In this work, we found that complexes **1a**, **2a**, **3**, **4a**, and **5a** all significantly facilitated the uptake of DAPI. As shown in Figure 11, in the absence of the gold(III)–porphyrin complexes, treatment of SUNE1 cells with DAPI for 2 h gave only a weak blue nuclear fluorescent signal. Co-incubation of DAPI with **1a** (0.056 μM), **3** (0.84 μM), and **5a** (0.091 μM) resulted in a marked enhancement of the blue fluorescent nuclear signal, which was clearly visualized.

Co-incubation of the cytotoxic complexes **1a**, **3**, and **5a** with DAPI at two different concentrations of 10 and 50 nM also significantly increased the cytotoxicity of these gold(III)–porphyrin complexes toward SUNE1 cancer cells (Table 6). The IC_{50} values of **1a**, **3**, and **5a** were found to be 0.023, 0.41, and 0.038 μM, respectively, with the co-incubation of DAPI at the 50 nM level. In contrast, there was no apparent synergistic, cytotoxic effect on SUNE1 cells observed upon the co-incubation of DAPI at the 50 nM level with **2a** (1.8 vs. 1.7 μM) or **4a** (82 vs. 73 μM).

Discussion

Lipophilic cations have previously been reported in the field of anticancer drug design.[33] Examples include the organic planar aromatic cations, such as terephthalanilide, which have a high binding affinity to the mitochondrial membrane. In this work, the ligation of dianionic porphyrinato ligands to gold(III) led to $[Au(Por)]^+$ complexes that are monocationic, lipophilic, and have a planar geometry.

The crystal structures of $[Au^{III}(TPP)]^+$ (**1a**), $[Au^{III}(p\text{-F-TPP})]^+$ (**1f**), and $[Au^{III}(p\text{-ph-TPP})]^+$ (**1g**) reveal that the cavity of the porphyrinato ligand is adequate to accommodate the gold(III) ion in a planar geometry. The N-Au-N angles found in **1a**, **1f**, and **1g** are close to 90°; whereas the related N-Au-N angles found in the gold(III) complexes of 1,4,8,11-tetraazacyclotetradecane (84.1–96.1°)[34] and 2,2′:6′,2″-terpyridine (81.2–81.5°)[35] significantly deviate from 90°. Thus, the porphyrin ligand scaffold is able to stabilize the gold(III) ion, which was also demonstrated by the stability tests.

In the literature, there are reports of hydrophobic/-philic substituents at the peripheral phenyl rings having a pronounced effect on the overall biological properties, such as anti-HIV activity.[36] In this work, we prepared gold(III)–porphyrin complexes with a wide range of lipophilic characteristics ($\log P = -1.85$ to $+1.95$). Cytotoxicity evaluation (MTT assay) revealed that Types I (**1a**–**1f**, **h**), III (**3**), and V (**5a** and **5c**–**g**) are highly cytotoxic with most of their IC_{50} values in the submicromolar range. The gold(III)–porphyrin complexes **1i**, **5a**, **5f**, and **5g** all have similar lipophilicity and their cytotoxicities are similar. Complex **1a** was preferentially cytotoxic to NPC cell lines (i.e., SUNE1, HK1, and HONE1). Complex **3** $[Au^{III}(OEP)]^+$ (H_2OEP = octaethylporphyrin) also exhibited potent cytotoxicity against all of the cancer cell lines examined.

The hydrophilic substituents render complexes **2a**–**2d**, **4a**, **4b**, **5b**, and **5c** able to exhibit a better aqueous solubility. Some of these substituents also significantly alter the overall cytotoxic activity. Microscopic examination, as well as flow cytometric analysis revealed that there was no apparent increase in the death of the SUNE1 cells after treatment with complexes **2a**–**2d** when compared with the vehicle control. Thus, complexes **2a**–**2d** are cytostatic instead of cytotoxic to cancer cells. The saccharide substituents result in the gold(III)–porphyrin complexes **2a**–**2d** having higher IC_{50} values than **1a**. More importantly, these complexes displayed selectivity toward cancer cells. As an example, the IC_{50} value of **2a** toward HONE1 cells is at least 83-fold lower than that toward normal lung fibroblast cells. In the literature, compounds with glycosylated ligands are known to inhibit specific cellular enzymes, such as glycosidase or cyclooxygenase-2.[37] In this work, the free porphyrin H_2(4-glucosyl-TPP) has also been found to display cytostatic properties toward SUNE1 cells. Unlike glycosylated porphyrinato li-

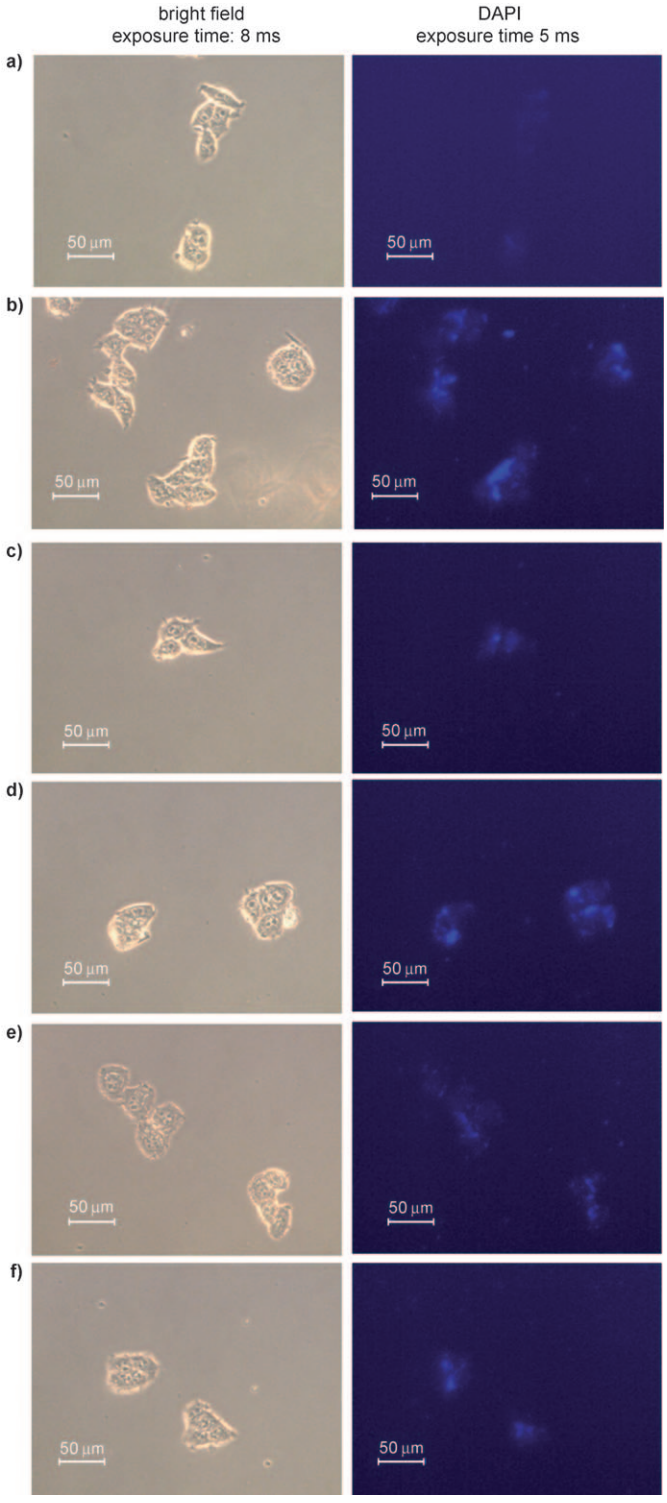

Figure 11. Bright-field and fluorescent images of a) vehicle control, b) **1a**-, c) **2a**-, d) **3**-, e) **4a**-, and f) **5a**-treated SUNE1 cells co-incubated with DAPI.

gands, both the charged *N*-methylpyridinyl (for **4a**) and sulfonyl (for **4b**) groups change the overall monocationic status of the $[Au(Por)]^+$ core, resulting in a significant reduction in cytotoxicity.

Table 6. In vitro cytotoxicity of the gold(III)–porphyrin complexes toward SUNE1 cells in the absence and presence of DAPI.

	IC_{50} [μM]		
Complex	without DAPI	with DAPI (10 nM)	with DAPI (50 nM)
1a	0.056 ± 0.007	0.037 ± 0.007	0.023 ± 0.007
2a	1.8 ± 0.4	2.0 ± 0.5	1.7 ± 0.2
3	0.84 ± 0.11	0.62 ± 0.13	0.41 ± 0.05
4a	82 ± 7	84 ± 7	73 ± 5
5a	0.091 ± 0.021	0.053 ± 0.009	0.038 ± 0.011
cisplatin	8.5 ± 1.1	6.9 ± 1.2	4.3 ± 0.3

The gold(III) tetraarylporphyrin complexes are among the most cytotoxic gold(III) complexes reported. Although $[Au^{III}(terpy)Cl]^{2+}$ (terpy = 2,2′:6′,2″-terpyridine) and its derivatives have been reported to display similar cytotoxicity to that of the gold(III)–porphyrin complexes described in this work, a parallel cytotoxicity study revealed that free terpy ligands are highly cytotoxic with IC_{50} values of about 0.5 μM.[6v] Shaw suggested that oxidative cytotoxicity, which is due to the Au^{III} to Au^{I} reduction is crucial for the anticancer action of most cytotoxic gold(III) complexes reported in the literature.[5i] Notwithstanding this, the gold(III) ion in $[Au(Por)]^+$ is tightly bound by the porphyrinato ligand, and the gold(III)–porphyrin complexes are stable against demetalation reactions and biological reduction (e.g., glutathione to glutathione disulfide).[9i] Thus, the cytotoxic mechanism of action of the gold(III)–porphyrin complexes does not necessarily involve the reduction of gold(III) to gold(I).

Lipophilicity is a crucial parameter in correlating the anticancer efficacy of different lipophilic cations. An increase in lipophilicity enhances the cellular uptake of the cations into cancer cells, and hence, improves their overall anticancer efficacies. As depicted in Figures 2 and 3, both the cytotoxicity and cellular uptake correlate with the lipophilicity of the gold(III)–porphyrin complexes. These results lend credibility to the hypothesis that gold(III)–porphyrin complexes exert their anticancer activities as organic lipophilic planar cations. However, the IC_{50} values of **1g**, **2a**, and **2c** deviate from the aforementioned correlations. The poor aqueous solubility of the highly lipophilic **1g** can account for its unexpected low cytotoxicity. The saccharide substituents in **2a** and **2c** may also lead to alternative modes of cytotoxic action.

To gain more insight into the modes of action of the gold(III)–porphyrin complexes, flow cytometric experiments using propidium iodide (PI) as the DNA staining reagent were conducted. Complexes **1a**, **2a**, **3**, and **5a** induced partial S-phase cell-cycle arrest, signifying an activation of cell-cycle checkpoints in response to DNA damage, which may contribute to the cytotoxicity of these complexes. For this reason, we examined the direct interactions between ctDNA and the gold(III)–porphyrin complexes (**1a**, **2a**, **3**, **4**, and **5a**) by means of UV/Vis absorption titration and gel mobility shift experiments. All of these complexes were found to have high binding constants similar to those of $[Ru^{II}(phen)_2dppz]^{2+}$ (phen = 1,10-phenanthroline and dppz = dipyridyl[3,2-*a*:2′3′-*c*]phenazine),[38] $[Pt^{II}(terpy)Cl]^+$,[39] and

$[Pt^{II}(terpy)(glycosylated\ arylacetylide)]^+$.[39] The gel mobility shift assay suggested that the cytotoxic complexes **1a**, **3**, and **5a** bind to DNA through a nonintercalating binding mode. It seems likely that these three gold(III) complexes neither stabilize the G-quadruplex nor inhibit the DNA topoisomerase reaction (Figures 7 and 8). In contrast, the cytostatic complex **2a** and the relatively nontoxic **4a** interacted with DNA in a manner similar to the DNA intercalator in the gel mobility shift assay, and impeded the DNA-binding protein, Topo I, from relaxing the supercoiled plasmid DNA. Notably, unlike the free porphyrins (e.g., $[H_2TMPyP]^{4+}$) and some of their metallo derivatives (e.g., complex **4a**),[27] we showed that the anticancer properties of the cytotoxic complexes **1a**, **3**, and **5**, and that of the cytostatic complex **2a**, did not involve the inhibition of telomerase or G-quadruplex stabilization.

We have also examined the interaction of the gold(III)–porphyrin complexes with potential protein targets. TrxR is known to be a potential cellular target for a variety of metal complexes, including gold(III) complexes.[5d] As revealed by in vitro assays, complexes **1a**, **2a**, and **3** inhibited TrxR. In mammalian TrxR, the redox center of the binding pocket consists of a selenocysteine redox pair that approaches the N-terminal active site of the other subunit for electron-transfer reactions.[40] Notably, the selenolate group at the active site, after reduction, shows a large propensity to interact with metal ions, rendering TrxR a likely pharmacological target for metal complexes. In the present study, the direct interaction of TrxR with **1a** was scrutinized by means of a computational molecular docking experiment. As described in the Results section, complex **1a** was found to favorably bind to the redox pocket of TrxR.

It has been documented that the mitochondrial binding event, the interaction with cellular DNA, and TrxR inhibition all participate in the induction of apoptosis in cancer cells by anticancer agents.[41] Apoptosis is typically accompanied by the activation of a class of death proteases (caspases).[24] In this work, the cytotoxic complexes **1a**, **3**, and **5a** markedly affected caspase-3 activation, whereas the glycosylated gold(III)–porphyrin **2a** and $[Au^{III}(TMPyP)]Cl_5$ (**4**) did not. As gold(III)–porphyrin complexes act as lipophilic cations, which tend to target mitochondria,[14,15] we focused on examining the expression level of a key mitochondrial-related protein, the anti-apoptotic bcl-2. This anti-apoptotic protein promotes cell survival by modulating mitochondrial factors involved in the activation of the downstream caspases that effect apoptosis in the cells. In this work, complex **1a** was found to induce apoptosis of SUNE1 cells, most likely by downregulating the anti-apoptotic proteins bcl-2. However, complex **1a** did not alter the expression level of another anti-apoptotic protein, that is, mcl-1. We also examined the likelihood of the binding of **1a** to bcl-2 as well as mcl-1 by using molecular docking (ICM) and the results reveal that **1a** favorably interacts with bcl-2, but interacts poorly with the structurally similar mcl-1.[42] In addition to **1a**, results of molecular-docking experiments revealed that the cytotoxic complexes **3** and **5a** also bind bcl-2. In contrast, complexes **2a** and **4a**, having, respectively, glycosylated and charged moieties at the periphery of the porphyrin ligand, had poor binding scores in the molecular-docking experiments, in line with their weaker cytotoxicity.

Angiogenesis, the formation of new blood vessels, is one of the integral parts of tumor growth and metastasis. Certain metal complexes, such as imidazolium *trans*-tetrachloro(dimethylsulfoxide)imidazoleruthenate(III) (NAMI-A), exhibit promising inhibitory effects toward solid tumors through an inhibition of angiogenesis.[43] Nevertheless, the anti-angiogenic activities of gold(III) complexes have not been explored. By means of an in vitro tube formation assay, we demonstrated that complexes **2a** and **3** significantly reduced endothelial cord formation in MS1 cells on Matrigel at subtoxic concentrations. This anti-angiogenic activity is not due to their cytotoxicity, since approximately 90% of the endothelial cells remained viable after 8 h incubation. Recently, Martin and co-workers showed that inhibition of Trx/TrxR is associated with the anti-angiogenic activity of a novel benzothiazole-substituted quinol compound (NSC 706704).[32] Thus, it is possible that **2a** and **3** inhibit angiogenesis through a similar mechanism.

A combination of chemotherapeutic agents for cancer treatment (e.g., cisplatin and 5-fluorouracil for nasopharyngeal carcinoma) is commonly employed in clinical settings. Thus, there is considerable interest in examining whether a potential drug lead can facilitate the uptake or exert a synergistic effect upon co-treatment with other cytotoxic agents. By fluorescence microscopic examination and making use of the fluorescent property of the DNA binding dye DAPI, complexes **1a**, **3**, and **5a** were shown to facilitate the cellular uptake of the fluorescent dye. The cytotoxic properties of these three gold(III)–porphyrin complexes were also enhanced in the presence of DAPI at subcytotoxic concentrations. Presumably, the lipophilic cationic gold(III)–porphyrin complexes may induce a subtle membrane permeabilization, thereby assisting delivery of nonpermeable compounds into the cells. This property may facilitate combination with other therapeutic agents in the development of anticancer gold(III)–porphyrin complexes.

Conclusion

We have developed a series of gold(III)–porphyrin complexes, which have promising anticancer activities. The biological properties of the gold(III)–porphyrin complexes **1a**, **2a**, **3**, **4a**, and **5a** are summarized in Table 7. DNA, bcl-2, and thioredoxin reductase (but not G-quadruplex or telomerase) are potential cellular targets of cytotoxic gold(III)–porphyrin complexes **1a**, **3**, and **5a**. Gold(III)–porphyrin complexes with saccharide conjugations (**2a**–**2d**) are not cytotoxic, but exhibit potent cytostatic activity and high selectivity toward cancer cells. Complexes **2a** and **3** are anti-angiogenic at their noncytotoxic concentrations. The cytotoxic complexes **1a**, **3**, and **5a** significantly enhance the cellular uptake of organic fluorescent dyes and a synergistic anti-

Table 7. Summary of the biological properties of complexes **1a**, **2a**, **3**, **4a**, and **5a**.

Complex	**1a**	**2a**	**3a**	**4a**	**5a**
average IC_{50} value to NPC [μM]	0.057	2.2	0.34	>81	0.091
highest cancer cell selectivity (IC_{50} ratio: CCD-19Lu/cancer cells)	5.7	>83	12	>1.9	3.2
mode of inhibition to cancer cells	cytotoxic	cytostatic	cytotoxic	relatively nontoxic	cytotoxic
binding constant to ctDNA [$dm^3 mol^{-1}$]	2.8×10^6	5.8×10^5	4.1×10^6	4.9×10^5	1.9×10^6
inhibition of PCR stop assay with G-quadruplex substrate	no	no	no	yes	no
inhibition of telomerase	no	no	no	yes	no
inhibition of Topo I-induced DNA relaxation	no	no	no	yes	no
downregulation of bcl-2 expression	yes	no	yes	no	yes
bcl-2 binding energy [kcal mol^{-1}]	−20	+14	−16	−11	−21
inhibition of thioredoxin reductase	yes	yes	yes	no	no
anti-angiogenic	n.d.[a]	yes	yes	no	n.d.[a]
synergism in cytotoxicity upon co-incubation with DAPI	yes	no	yes	no	yes

[a] n.d. = not determined.

cancer effect was observed upon co-treatment with the DNA-binding dye, DAPI. It is apparent that ligation of porphyrinato ligands to the gold(III) ion gives a family of lipophilic planar cations $[Au(Por)]^+$, which have tunable properties. All of these biological properties and the ease of structural modification of the gold(III)–porphyrins warrants that $[Au(Por)]^+$ is a feasible choice for the development of future therapeutic applications.

Experimental Section

Materials: All chemicals, unless otherwise noted, were purchased from Sigma–Aldrich. All solvents were purified according to conventional methods. ctDNA was purified by phenol/chloroform extraction. The Cell Proliferation Kit I (MTT) and the In Vitro Angiogenesis Kit were purchased from Roche.

Instrumentation: ^{1}H NMR spectra were recorded on a DPX 300 or 400 Bruker FT-NMR spectrometer with chemical shifts reported (in ppm) relative to tetramethylsilane (TMS). Mass spectra (FAB or EI) were recorded on a Finnigan MAT95 mass spectrometer by using 3-nitrobenzyl alcohol (NBA) as the matrix. ESI mass spectra were recorded on a Finnigan LCQ mass spectrometer. Gold analysis was undertaken by using an Agilent 7500 inductively coupled plasma mass spectrometer. All absorption spectra were recorded on a Perkin–Elmer Lambda 900 UV/Vis spectrophotometer. Elemental analyses were performed by the Institute of Chemistry at the Chinese Academy of Sciences, Beijing. Flow cytometric analysis was performed with a Coulter EPICS flow cytometer (Coulter, Miami, FL) equipped with 480 long, 525 band, and 625 long pass mirrors.

The synthesis and characterization of **1a**–**1e**,[9h] **4a**, and **4b**[9g] have been reported previously.

[Au(TPP-F_4)]Cl (***1f***): Yield: 54%; ^{1}H NMR (300 MHz, $CDCl_3$, 25°C, TMS): δ = 9.24 (s, 8H), 8.31 (s, 8H), 7.72–7.43 ppm (m, 8H); UV/Vis (DMSO): λ_{max} ($\log\varepsilon$) = 410 (5.36), 527 nm (4.30 $mol^{-1} dm^3 cm^{-1}$); MS (FAB): *m/z*: 881 [M^+]; elemental analysis calcd (%) for $C_{44}H_{24}N_4ClF_4Au$: C 57.62, H 2.64, N 6.11; found: C 57.87, H 2.70, N, 6.01.

[Au(TPP-Ph_4)]Cl (***1g***): Yield: 46%; ^{1}H NMR (300 MHz, $CDCl_3$, 25°C, TMS): δ = 9.40 (s, 8H), 8.35 (d, *J* = 8.1 Hz, 8H), 8.11 (d, *J* = 8.1 Hz, 8H), 7.93 (d, *J* = 7.2 Hz, 8H), 7.63 (t, *J* = 7.4 Hz, 8H), 7.52 ppm (t, *J* = 7.4 Hz, 4H); UV/Vis (DMSO): λ_{max} ($\log\varepsilon$) = 421 (5.50), 529 nm (4.43 $mol^{-1} dm^3 cm^{-1}$); MS (FAB): *m/z*: 1114 [M^+]; elemental analysis calcd (%) for $C_{68}H_{44}N_4ClAu$: C 71.05, H 3.86, N 4.87; found: C 69.32, H 4.09, N, 4.57.

[Au(TPP-$(OAc)_4$)]Cl (***1h***): Yield: 57%; ^{1}H NMR (300 MHz, $CDCl_3$, 25°C, TMS): δ = 9.21 (s, 8H), 8.51 (d, *J* = 8.2 Hz, 8H), 8.39 (d, *J* = 8.2 Hz, 8H), 4.12 ppm (s, 12H); UV/Vis (DMSO): λ_{max} ($\log\varepsilon$) 413 (5.53), 525 nm (4.32 $mol^{-1} dm^3 cm^{-1}$); MS (FAB): *m/z*: 1042 [M^+]; elemental analyses calcd (%) for $C_{50}H_{33}N_4O_6ClAu$: C 58.98, H 3.27, N 5.50; found: C 58.74, H 3.14, N, 5.04.

[Au(TPP-$(OMe)_4$)]Cl (***1i***): Yield: 63%; ^{1}H NMR (300 MHz, $CDCl_3$, 25°C, TMS): δ = 9.36 (s, 8H), 7.57 (s, 8H), 4.19 (s, 12H), 3.98 ppm (s, 24H); UV/Vis (CH_2Cl_2): λ_{max} ($\log\varepsilon$) 423 (5.18), 526 nm (4.17 $mol^{-1} dm^3 cm^{-1}$); MS (FAB): *m/z*: 1169 [M^+]; elemental analysis calcd (%) for $C_{56}H_{52}N_4O_{12}ClAu$: C 55.80, H 4.35, N 4.65; found: C 55.56, H 4.28, N, 4.57.

*[Au(TPP-*R,R-*saccarideOH)]Cl* (***2a***): Yield: 54%; ^{1}H NMR (400 MHz, CD_3OD, 25°C, TMS): δ = 9.39 (s, 8H), 8.18 (d, *J* = 8.5 Hz, 8H), 7.63 (d, *J* = 8.6 Hz, 8H), 5.30 (d, *J* = 7.2 Hz, 4H), 4.01 (d, *J* = 10.1 Hz, 4H), 3.81 (dd, *J* = 5.8, 6.2 Hz, 4H), 3.71–3.47 ppm (m, 16H); UV/Vis (H_2O): λ_{max} ($\log\varepsilon$) 408 (4.78), 531 nm (3.51 $mol^{-1} dm^3 cm^{-1}$); MS (ESI): *m/z*: 1521.3 [M^+]; elemental analysis calcd (%) for $C_{68}H_{68}N_4O_{24}ClAu$: C 52.43, H 4.40, N 3.60; found: C 49.76, H 4.72, N 3.49.

*[Au(TPP-*R,R-*saccarideOAc)]Cl* (***2b***): Yield: 72%; ^{1}H NMR (400 MHz, $CDCl_3$, 25°C, TMS): δ = 9.26 (s, 8H), 8.23 (d, *J* = 8.5 Hz, 8H), 7.46 (d, *J* = 8.6 Hz, 8H), 5.50–5.43 (m, 12H), 5.30 (m, 4H), 4.43 (dd, *J* = 5.5, 7.0 Hz, 4H), 4.30 (dd, *J* = 2.0, 10.2 Hz, 4H), 4.10–4.06 (m, 4H), 2.22 (s, 12H), 2.11 ppm (d, *J* = 6.2 Hz, 36H); UV/Vis (DMSO): λ_{max} ($\log\varepsilon$) 419 (5.22), 529 nm (4.05 $mol^{-1} dm^3 cm^{-1}$). MS (FAB): *m/z*: 2194 [M^+]; elemental analysis calcd (%) for $C_{100}H_{100}N_4O_{40}ClAu$: C 53.85, H 4.52, N 2.51; found: C 52.58, H 4.63, N 2.61.

*[Au(TPP-*R,L-*saccarideOH)]Cl* (***2c***): Yield: 61%; ^{1}H NMR (400 MHz, CD_3OD, 25°C, TMS): δ = 9.31 (s, 8H), 8.10 (d, *J* = 8.4 Hz, 8H), 7.64 (d, *J* = 8.7 Hz, 8H), 5.27 (d, *J* = 7.7 Hz, 4H), 4.02 (dd, *J* = 7.5, 2.6 Hz, 8H), 3.90 (m, 12H), 3.75 ppm (dd, *J* = 3.4, 6.3 Hz, 4H); UV/Vis (H_2O): λ_{max} ($\log\varepsilon$) 408 (4.78), 531 nm (3.51 $mol^{-1} dm^3 cm^{-1}$); MS (ESI): *m/z*: 1521.3 [M^+]; elemental analysis calcd (%) for $C_{68}H_{68}N_4O_{24}ClAu$: C 52.43, H 4.40, N 3.60; found: C 50.89, H 4.65, N, 3.48.

*[Au(TPP-*R,L-*saccarideOAc)]Cl* (***2d***): Yield: 78%; ^{1}H NMR (400 MHz, $CDCl_3$, 25°C, TMS): δ = 9.28 (s, 8H), 8.22 (d, *J* = 8.4 Hz, 8H), 7.48 (d, *J* = 8.5 Hz, 8H), 5.71 (dd, *J* = 7.9, 2.6 Hz, 4H), 5.58 (d, *J* = 3.4 Hz, 4H), 5.46 (d, *J* = 7.9 Hz, 4H), 5.28 (dd, *J* = 3.4, 7.1 Hz, 4H), 4.39 (m, 4H), 4.28 (m, 8H), 2.27 (s, 12H), 2.24 (s, 12H), 2.09 ppm (d, *J* = 4.4 Hz, 24H); UV/Vis (DMSO): λ_{max} ($\log\varepsilon$) 419 (5.22), 529 nm (4.05 $mol^{-1} dm^3 cm^{-1}$); MS (FAB): *m/z*: 2194 [M^+]; elemental analysis calcd (%) for $C_{100}H_{100}N_4O_{40}ClAu$: C 53.85, H 4.52, N 2.51; found: C 50.13, H 4.51, N 2.38.

[Au(OEP)]Cl (***3***): Yield: 62%; ^{1}H NMR (300 MHz, $CDCl_3$, 25°C, TMS): δ = 10.51 (s, 8H), 7.89 (s, 4H), 2.10 (t, *J* = 6.8 Hz, 24H), 1.59 ppm (q, *J* = 5.8 Hz, 16H); UV/Vis (CH_2Cl_2): λ_{max} ($\log\varepsilon$) 389 (5.35), 510 (3.98), 545 nm (4.23 $mol^{-1} dm^3 cm^{-1}$); MS (FAB): *m/z*: 731 [M^+]; elemental analysis calcd (%) for $C_{36}H_{44}N_4ClAu$: C 56.51, H 5.80, N 7.32; found: C 56.14, H 5.67, N 7.58.

[Au(TPP-OMe)]Cl (***5a***): Yield: 61%; ^{1}H NMR (300 MHz, $CDCl_3$, 25°C, TMS): δ = 9.34 (d, *J* = 5.2 Hz, 2H), 9.29 (d, *J* = 5.1 Hz, 6H), 8.23 (d, *J* = 7.9 Hz, 6H), 8.16 (d, *J* = 8.6 Hz, 2H), 7.92–7.85 (m, 9H), 7.39 ppm (d, *J* = 8.6 Hz, 2H); UV/Vis (DMSO): λ_{max} ($\log\varepsilon$) 415 (5.28), 525 nm

($4.18\ mol^{-1}dm^3cm^{-1}$); MS (FAB): m/z: 840 [M^+]; elemental analysis calcd (%) for $C_{45}H_{30}N_4OClAu$: C 61.76, H 3.46, N 6.40; found: C 61.80, H 3.58, N 6.26.

[Au(TPP-OCH$_2$COOH)]Cl (***5b***): Yield: 71%; ^{1}H NMR (300 MHz, $CDCl_3$, 25°C, TMS): δ = 9.29–9.11 (m, 8H), 8.31–8.27 (m, 8H), 7.88–7.74 (m, 9H), 7.50 (d, J = 8.6 Hz, 2H), 5.29 ppm (s, 2H); UV/Vis (DMSO): λ_{max} ($\log\varepsilon$) 414 (5.15), 528 nm ($4.13\ mol^{-1}dm^3cm^{-1}$); MS (FAB): m/z: 884 [M^+]; elemental analysis calcd (%) for $C_{46}H_{30}N_4O_3ClAu$: C 60.11, H 3.29, N 6.10; found: C 59.14, H 3.68, N 6.35.

[Au(TPP-O(CH$_2$)$_4$COOH)]Cl (***5c***): Yield: 62%; ^{1}H NMR (400 MHz, $CDCl_3$, 25°C, TMS): δ = 9.24 (dd, J = 5.0, 13.5 Hz, 8H), 8.20 (dd, J = 7.0, 19.6 Hz, 8H), 7.89–7.79 (m, 9H), 7.3 (d, J = 8.5 Hz, 2H), 4.30 (s, 2H), 2.63–2.60 (m, 2H), 2.05 ppm (s, 4H); UV/Vis (DMSO): λ_{max} ($\log\varepsilon$) 415 (5.31), 528 nm ($4.25\ mol^{-1}dm^3cm^{-1}$); MS (FAB): m/z: 925 [M^+]; elemental analysis calcd (%) for $C_{49}H_{36}N_4O_3ClAu$: C, 61.22; H, 3.77; N, 5.83; found: C 59.93, H 3.57, N 5.49.

[Au(TPP-OBu)]Cl (***5d***): Yield: 48%; ^{1}H NMR (400 MHz, $CDCl_3$, 25°C, TMS): δ = 9.36 (d, J = 5.2 Hz, 2H), 9.28 (d, J = 4.1 Hz, 6H), 8.23 (d, J = 7.7 Hz, 6H), 8.13 (d, J = 8.6 Hz, 2H), 7.94–7.84 (m, 9H), 7.38 (d, J = 8.6 Hz, 2H), 4.28 (t, J = 6.4 Hz, 2H), 2.01–1.96 (m, 2H), 1.17–1.09 ppm (m, 5H); UV/Vis (DMSO): λ_{max} ($\log\varepsilon$) 414 (5.33), 527 nm ($4.21\ mol^{-1}dm^3cm^{-1}$); MS (FAB): m/z: 882 [M^+]; elemental analysis calcd (%) for $C_{48}H_{36}N_4OClAu$: C 62.85, H 3.96, N 6.11; found: C 62.98, H 3.99, N 6.20.

[Au(TPP-OOct)]Cl (***5e***): Yield: 36%; ^{1}H NMR (400 MHz, $CDCl_3$, 25°C, TMS): δ = 9.34 (d, J = 5.2 Hz, 2H), 9.27 (d, J = 4.0 Hz, 6H), 8.24 (d, J = 7.8 Hz, 6H), 8.15 (d, J = 8.6 Hz, 2H), 7.91–7.83 (m, 9H), 7.37 (d, J = 8.6 Hz, 2H), 4.27 (t, J = 6.5 Hz, 2H), 2.02–1.97 (m, 2H), 1.38–1.31 ppm (m, 13H); UV/Vis (DMSO): λ_{max} ($\log\varepsilon$) 413 (5.29), 528 nm ($4.23\ mol^{-1}dm^3cm^{-1}$); MS (FAB): m/z: 938 [M^+]; elemental analysis calcd (%) for $C_{52}H_{44}N_4OClAu$: C 64.17, H 4.56, N 5.76; found: C 64.24, H 4.43, N 5.84.

[Au(3,5-OMeTPP)]Cl (***5f***): Yield: 60%; ^{1}H NMR (400 MHz, $CDCl_3$, 25°C, TMS): 9.37 (d, J = 5.2 Hz, 2H), 9.25 (d, J = 3.6 Hz, 6H), 8.24 (d, J = 7.9 Hz, 6H), 7.91–7.84 (m, 9H), 7.44–7.43 (m, 2H), 6.97 (s, 1H), 3.98 ppm (s, 6H); UV/Vis (DMSO): λ_{max} ($\log\varepsilon$) 414 (5.43), 526 nm ($4.33\ mol^{-1}dm^3cm^{-1}$); MS (FAB): m/z: 870 [M^+]; elemental analysis calcd (%) for $C_{46}H_{32}N_4O_2ClAu$: C 61.04, H 3.56, N 6.19; found: C 62.49, H 3.64, N 6.24.

[Au(TPP-3,4-OMe)]Cl (***5g***): Yield: 71%; ^{1}H NMR (400 MHz, $CDCl_3$, 25°C, TMS): δ = 9.35 (d, J = 5.2 Hz, 2H), 9.27 (d, J = 6.1 Hz, 6H), 8.24–8.22 (m, 6H), 7.91–7.79 (m, 11H), 7.34 (d, J = 8.1 Hz, 1H), 4.20 (s, 3H), 4.00 ppm (s, 3H); UV/Vis (DMSO): λ_{max} ($\log\varepsilon$) 412 (5.26), 528 nm ($4.24\ mol^{-1}dm^3cm^{-1}$); MS (FAB): m/z: 870 [M^+]; elemental analysis calcd (%) for $C_{46}H_{32}N_4O_2ClAu$: C 61.04, H 3.56, N 6.19; found: C 60.58, H 3.71, N 6.14.

X-ray crystal structure: X-ray crystal structures of [Au^{III}(TPP)](ClO_4) (CCDC-201191)[9i], [Au^{III}(*p*-F-TPP)](Au^{I}Cl$_2$) (CCDC-738028) and **1g** (CCDC-738027) are shown in the Supporting Information, Figures S13–S15, respectively. These data can be obtained free of charge from The Cambridge Crystallographic Data Centre via www.ccdc.cam.ac.uk/data_request/cif. Crystals of [Au^{III}(TPP)]ClO_4 were obtained by slow evaporation of a solution in DMSO, crystals of [Au^{III}(*p*-F-TPP)](Au^{I}Cl$_2$) were obtained by slow diffusion of Et_2O into a solution of [Au^{III}(*p*-F-TPP)](Au^{I}Cl$_2$) in DMF, and crystals of **1g** were obtained by slow diffusion of Et_2O into a solution of **1g** in CH_3CN.

Diffraction experiments were performed on a MAR diffractometer by using graphite monochromatized $Mo_{K\alpha}$ radiation (λ = 0.71073 Å). The images were interpreted and intensities integrated by using the program DENZO. The structure was solved by direct methods by employing the SHELXS-97[44] program on a PC. Au was located according to the direct method. The positions of the other non-hydrogen atoms were found after successful refinement by the full-matrix least-squares method by using the program SHELXL-97 on a PC. For [Au^{III}(TPP)](ClO_4), one crystallographic asymmetric unit consists of half of a formula unit. In the final stage of least-squares refinement, all non-hydrogen atoms were refined anisotropically. For [Au^{III}(*p*-F-TPP)](Au^{I}Cl$_2$), one crystallographic asymmetric unit consists of one formula unit, including a gold(I) dichloride anion. In the final stage of least-squares refinement, disordered oxygen atoms were refined isotropically and other non-hydrogen atoms anisotropically. For **1g**, one crystallographic asymmetric unit consists of one formula unit, including one chloride anion and one DMF molecule. In the final stage of least-squares refinement, all non-hydrogen atoms were refined anisotropically.

Measurement of lipophilicity: Lipophilicity was determined by measuring log*P* by using a shake-flask method.[21] Saturated *n*-octanol with sodium chloride (organic phase) was prepared by mixing it with an equal volume of an aqueous solution of sodium chloride (0.9% w/v) at 45 rpm for one week. The organic phase was collected and each type of gold(III)–porphyrin complex was dissolved at a final concentration of 25 μM in the organic phase. An equal volume of an aqueous solution of sodium chloride (0.9% w/v) was added and the solutions were mixed for 30 min at 45 rpm. Samples were centrifuged (1500 *g*, 10 min) and the content of gold(III)–porphyrin complexes in the organic and aqueous phases was determined by measuring the absorbance at the λ_{max} for each complex. Log*P* was defined as the logarithmic ratio of drug concentrations in the organic and aqueous phases.

Cell lines and cell culture: Human normal lung fibroblast (CCD-19Lu) and MS1 (CRL-2279) cell lines were commercially obtained from American Type Culture Collection (ATCC, Rockville, MD, USA). Human nasopharyngeal carcinoma cells (HONE1, SUNE1, and its cisplatin-resistant variant, CNE1) were generously provided by Prof. S. W. Tsao (Department of Anatomy, The University of Hong Kong). Cell-culture flasks and 96-well microtitre plates were purchased from Nalge Nunc. Culture medium, other medium constituents, and PBS were purchased from Gibco BRL.

The HeLa and CCD-19Lu cells were maintained in a minimum essential medium (MEM) with Earle's balanced salts. The HepG2 and MS1 cells were maintained in a minimum essential medium (DMEM) with a D-glucose content of 4500 $mg\,L^{-1}$. The SUNE1, CNE1, and HONE1 cells were maintained in RPMI 1640 medium. All the media were supplemented with L-glutamine (2 mM) and fetal bovine serum (10%). Penicillin (100 $U\,mL^{-1}$) and streptomycin (100 $\mu g\,mL^{-1}$) were added to all media. Cultures were incubated at 37°C in a humidified atmosphere of 5% CO_2/95% air, and were subcultured three times a week.

Cytotoxicity evaluation: Assays of cytotoxicity were conducted in 96-well, flat-bottomed microtitre plates. The supplemented culture medium (90 μL) with cells (1×10^5 cells mL^{-1}) was added to the wells. Gold(III)–porphyrin complexes were dissolved in the culture medium with 1% DMSO to concentrations of 0.5–1 μM, and aliquots of the solutions were subsequently added to a set of wells. Cells for control experiments were treated with supplemented media with 1% DMSO (100 μL). The microtitre plates were incubated at 37°C in a humidified atmosphere of 5% CO_2/95% air for a further 3 d. All the assays were run in parallel with a negative control (i.e., vehicle control) and a positive control, in which cisplatin was used as a cytotoxic agent.

Assessment of cytotoxicity was carried out by using a modified method of the Mosmann-based MTT assay.[19] At the end of each incubation period, MTT solution (10 μL, Cell Proliferation Kit I, Roche) was added to each well and the cultures were incubated for a further 4 h at 37°C in a humidified atmosphere of 5% CO_2/95% air. A solubilizing solution (100 μL) was added into the wells to lyse the cells and to solublize the formazan complex formed. The microtitre plates were maintained in a dark, humidified chamber overnight. The formation of formazan was measured by using a microtitre plate reader at 550 nm and the percentages of cell survival were determined. The cytotoxicity was evaluated based on the percentage cell survival in a dose-dependent manner relative to the negative control.

Cellular-uptake experiments: Cellular-uptake experiments were conducted according to the literature method. In general, SUNE1 cells (5×10^4 cells) were seeded in 60 mm tissue-culture dishes with culture medium (2 $mL\,well^{-1}$) and incubated at 37°C in a humidified atmosphere of 5% CO_2/95% air for 24 h. The culture medium was removed and replaced with a medium containing the gold(III) complexes. After exposure to the gold(III) complexes for 2 h, the medium was removed and the cell

monolayer was washed four times with ice-cold PBS. Milli-Q water (500 μL) was added and the cell monolayer was scraped off from the culture dish. Samples (300 μL) were digested in 70% HNO_3 (500 μL) at 70°C for 2 h then diluted 1:100 in water for inductively coupled plasma mass spectrometry (ICP MS) analysis.

Cell-cycle analysis: The SUNE1 cells were seeded at a density of 1×10^6 cells dish^{-1} in 6 cm culture dishes and incubated at 37°C in a humidified atmosphere of 5% CO_2/95% air for 24 h. The cells were left untreated or treated with gold(III)–porphyrin complexes (**1a** or **2a**) or cisplatin (5 μM, positive control), for 24 and 48 h. At the end of the incubation period, the cells were trypsinized, washed twice with ice-cold PBS, and fixed in 70% ice-cold ethanol. Cells were rehydrated in PBS and stained in a propidium iodide solution (50 μg mL^{-1}) containing RNase A (5 U mL^{-1}) for 30 min. 30000 events from each sample were counted in a flow cytometry. The data was analyzed by using Modfit 3.0 software.

Hemolysis: Human blood was collected in heparinized tubes and centrifuged at 1500 rpm for 10 min to isolate red blood cells. The cells were washed three times with PBS and resuspended in PBS. The cells were stored at 4°C and used within 3 h after collection. In a 48-well plate, gold(III)–porphyrin complexes (200 μL) were added to the warmed erythrocyte suspension and incubated for 30 min at 37°C. Final concentrations of the gold(III)–porphyrin complexes were 0.5 and 5 μM in triplicate. After incubation, the mixtures were spun at 1500 rpm for 2 min. The supernatants were transferred to clean curvettes and the absorbance was recorded at 540 nm. The percentage of hemolysis was calculated by using Equation (2):

$$\%\ \text{Hemolysis} = (\text{Abs}_{\text{sample}} - \text{Abs}_{-\text{ve}})/(\text{Abs}_{\max} - \text{Abs}_{-\text{ve}}) \times 100\,\% \qquad (2)$$

in which $\text{Abs}_{\text{sample}}$ is the average absorbance of supernatant from the samples, $\text{Abs}_{-\text{ve}}$ is the level of spontaneous hemolysis (Abs of supernatant taken from untreated samples). $\text{Abs}_{\max}$ is the maximum Abs (Abs of uncentrifuged mixture of the untreated samples).

Thioredoxin reductase assay: Inhibition of thioredoxin reductase activity by gold(III)–porphyrin complexes was quantified by the change in absorbance (vs. vehicle control) at 412 nm of 5,5′-dithiobis-2-nitrobenzoic acid (DTNB) to thionitrobenzoic acid.[45] In general, a solution of gold(III)–porphyrin complex (dissolved in DMSO as a 100× stock solution) was incubated with thioredoxin reducatase (1 μg) in potassium phosphate buffer (pH 7.0) containing ethylenediaminetetraacetic acid (EDTA, 1 mM), bovine serum albumin (0.2 mg mL^{-1}) and nicotinamide adenine dinucleotide phosphate (NADPH, 0.2 mM). After 1 h, DTNB dissolved in DMSO as a 100× stock solution (300 mM) was added. The reduction of DTNB in the presence or absence of the gold(III)–porphyrin complexes was measured over 2 min, and the extinction coefficient of thionitrobenzoic acid at 412 nm was taken as 13600 M^{-1} cm^{-1}.[46]

Absorption titration experiments: A solution of gold(III) complex (**1a**, **2a**, **3**, **4a**, or **5a**) in TBS/DMSO (9:1) solution (1 mL) was placed in a thermostatic cuvette and its absorption spectrum was recorded. Aliquots of a millimolar stock solution of ctDNA were added to the sample solution. The absorption spectra were recorded after equilibration for 1 min per aliquot until the saturation point was reached. The binding constant was determined by applying the Scatchard equation: $[\text{DNA}]/\Delta\varepsilon_{\text{ap}} = [\text{DNA}]/\Delta\varepsilon + 1[1/(\Delta\varepsilon\times K_{\text{b}})]$, in which $\Delta\varepsilon_{\text{ap}} = |\varepsilon_{\text{A}} - \varepsilon_{\text{B}}|$, $\varepsilon_{\text{A}} = A_{\text{obs}}/[\text{complex}]$, $\Delta\varepsilon = |\varepsilon_{\text{B}} - \varepsilon_{\text{F}}|$, and ε_{B} and ε_{F} correspond to the extinction coefficients of the DNA-bound and -unbound complex, respectively.

Gel mobility shift assay: A 100 base pair DNA ladder (corresponding to 15 μM in base pairs) was incubated with ethidium bromide, **1a**, **2a**, **3**, **4a**, or **5a** in a 1:1 ratio of DNA base pair to the complex for 30 min. The mixtures were analyzed by gel electrophoresis by using a 2% (w/v) agarose gel and tris-acetate-EDTA (TAE) buffer. The gel was immersed in an ethidium bromide solution after electrophoresis, and visualized by using UV transillumination.

Viscosity measurement: The method used by Suh and Chaires was employed in this study.[47] Viscosity experiments were performed by using a Cannon–Manning Semi-Micro Viscometer, immersed in a thermostated water bath maintained at 27°C. Titrations of **1a**, **2a**, **3**, **4a**, **5a**, ethidium bromide (EB), and Hoechst 33342 (H33342) were carried out by the addition of small volumes of concentrated stock solutions to the DNA sample in BPE buffer (Na_2HPO_4, 6 mM; NaH_2PO_4, 2 mM; Na_2EDTA, 1 mM) at pH 7.0 in the viscometer. Solutions in the viscometer were mixed by bubbling nitrogen through the solution. DNA concentrations of approximately 1 mM (in base pairs) were used.

Topoisomerase I inhibition assay: Plasmid DNA (2.9 kb) was purchased from Promega (Madison, WI, USA) at a concentration of 1 μg mL^{-1}. It was diluted to the working concentration in the reaction buffer (50 mM Tris/HCl (pH 7.5), 20 mM KCl, 1 mM EDTA, 0.3 mg mL^{-1} bovine serum albumin (BSA) and 1 mM dithiothreitol). Recombinant Topo I was kindly provided by Prof. Y. C. Cheng (Pharmacology, Yale University). Supercoiled (SC) plasmid DNA was diluted in reaction buffer to a concentration of 25 ng μL^{-1}. An aliquot of **1a**, **2a**, **3**, **4a**, or **5a** (1 μL) dissolved in PBS/EtOH (19:1, v/v), CPT, or vehicle control was added to a 75 ng of SC DNA dilution. The mixtures were incubated for 20 min at RT and Topo I solution (2 μL) was added. This solution was incubated at 37°C for 2 h. The reaction was terminated by addition of a 20% SDS solution (1.25 μL) and proteinase K (2.5 μL, 1 mg mL^{-1}). After incubation at 45°C for 1 h, the samples were analyzed by gel electrophoresis by using 1% (w/v) agarose gels containing 0.1% (w/v) SDS. The gel was stained by immersion into a bath of EB after electrophoresis and was visualized under UV illumination.

PCR stop assay: This experiment was performed according to the literature procedure.[28] A quadruplex-forming DNA sequence Pu27 (5′-TGGGGAGGGTGGGGAGGGTGGGGAAGG-3′) and its complementary sequence were employed in this study. The reactions were performed in a PCR buffer containing 10 μM of each pair of oligomers, dNTP (0.16 mM), *Taq* polymerase (2.5 U), and with gold(III)–porphyrin complexes (**1a** (0.056 μM), **2a** (1.8 μM), **3** (0.84 μM), **4a** (82 μM), and **5a** (0.091 μM). The PCR cycling conditions were 94°C for 3 min, followed by 30 cycles of 94°C for 30 s, 58°C for 30 s, and 72°C for 30 s. Amplified products were resolved on 15% nondenaturing polyacrylamide gels in Tri/borate/EDTA (TBE) buffer and stained with SYBR Green I.

Telomerase-inhibition assay: A photometric enzyme immunoassay, TeloTAGGG Telomerase PCR ELISA$^{\text{PLUS}}$ (Roche) for quantitative determination of teleomerase activity was employed and the assays were conducted by following the manufacturer's instruction. In essence, gold(III)–porphyrin complexes with doses corresponding to their cytotoxic IC_{50} values for SUNE1 cells (**1a** (0.056 μM), **2a** (1.8 μM), **3** (0.84 μM), **4a** (82 μM), and **5a** (0.091 μM) and a positive control $[H_2TMPyP]^{4+}$ (100 μM) were separately incubated with telomerase for 10 min at 37°C. The treated enzymes added telomeric repeats (TTAGGG) to the 3′ end of the biotin-labeled synthetic primer and the resultant conjugated PCR products were quantified by an ELISA plate reader with a 450 nm filter.

Western-blot analysis: SUNE1 cells were first treated with **1a** for 8 h. After washing with PBS, 2×10^6 cells were lysed in radio-immunoprecipitation assay (RIPA) buffer (100 μL, 1% Trition X-100, 10% deoxycholate, 50 mM Tris-HCl pH 7.5, 150 mM NaCl, 0.1% SDS, 0.1 mM PMSF, 10 μg mL^{-1} leupeptin, 10 μg mL^{-1} aprotinin) at 0°C. After centrifugation, the supernatants were collected. The cellular protein content was quantified by the DC Protein Assay (Bio-Rad). For detection, samples (15 μg lane^{-1}) were fractionated on a 12.5% SDS–PAGE in a Tris-Glycine running buffer and blotted on polyvinylidene fluoride (PVDF) membranes. The membrane was stained with red Ponceau and the gel was stained with Coomassie blue to check the loading homogeneity and transfer efficiency. The PVDF membranes were blocked overnight at room temperature in PBS containing 5% non-fat milk powder. Afterwards, the blots were incubated at RT for an hour with the primary antibody diluted in PBS containing 0.5% non-fat milk powder. Mouse polyclonal anti-bcl-2 and anti-bcl-xL were used as primary antibodies at 1:500 dilutions. After washing with PBS twice, the membranes were then incubated with the respective peroxidase-conjugated secondary antibody for an hour. Detection was performed by using the chemiluminescence procedure (ECL, Amersham).

Molecular dockings: A molecular model study on the interaction between the gold(III) complex and a specific protein target was performed. This was achieved by using Gaussian 03.[48] The gold complex was optimized by using DFT with a LanL2MB basis set.[49] The optimized struc-

ture of the platinum complex was used to do the docking. Molecular docking was performed by using the ICM-Pro 3.6–1 program (Molsoft).[50] According to the ICM method, the molecular system was described by using internal coordinates as variables. The biased probability Monte Carlo (BPMC) minimization procedure was used for global energy optimization. The BPMC global energy optimization method consists of the following steps: 1) a random conformation change of the free variables according to a predefined continuous probability distribution; 2) local energy minimization of analytical differentiable terms; 3) calculation of the complete energy including nondifferentiable terms, such as entropy and solvation energy; 4) acceptance or rejection of the total energy based on the Metropolis criterion and return to step 1. A series of five grid potential representations of the receptor were automatically generated and superimposed, which accounted for the hydrophobicity, carbon- and hydrogen-based van der Waals boundaries, hydrogen-bonding profile, and the electrostatic potential. The bindings between gold(III)–porphyrin complexes with bcl-2, mcl-1, and thioredoxin reductase were evaluated by a binding energy that reflects the quality of the complex. In the docking analysis the binding site was assigned across the entire protein molecule. Hydrogen and missing heavy atoms were added to the receptor structure followed by local minimization by using the conjugate gradient algorithm and analytical derivatives in the internal coordinates. The ICM docking was performed to find the most favorable orientation. The resulting gold(III)–porphyrin–protein complex trajectories were energy minimized, and the energies were computed.

Tube-formation assay: By using the In Vitro Angiogenesis Kit (Cayman Chemical), 10× Diluent Buffer and ECMatrix solution were mixed in a ratio of 1:9. The mixture (50 μL) was transferred to each well of a 96-well plate and incubated at 37 °C to allow for polymerization. After 1 h, MS1 cells (50000) premixed with **2a** (1.8 μM), **3** (0.84 μM), **4a** (82 μM), or **5a** (0.091 μM) in 100 μL of DMEM medium at different concentrations were added to the top of the polymerized matrix. After incubation at 37 °C for 8 h, tube formation in each case was examined under an inverted light microscope at 100× and 400× magnifications, and was quantified by using the Sigma Scan Pro software. The percentage of inhibition was calculated based on the distance measured relative to the untreated control.

Fluorescence microscopic examination: SUNE1 cells grown in a one-chamber slide (Nalgene; Nunc) were incubated with DAPI (20 nM) in the presence of **1a** (0.056 μM) **2a** (1.8 μM), **3** (0.84 μM), **4a** (82 μM), **5a** (0.091 μM), or DMSO for 2 h. The bright-field (fixed exposure time: 8 ms) and fluorescent (fixed exposure time: 5 ms) images were examined in Axiovert 200 (Carl Zeiss) and in an Axio Vision Rel. 4.5 imaging system (Carl Zeiss).

Acknowledgements

We acknowledge support from The University of Hong Kong (University Development Fund) and the Area of Excellence Scheme (AoE/P-10/01) administered by the University Grants Council (HKSAR, China). We thank Dr. Fuyi Zhang for the preparation of glycosylated porphyrins.

[1] a) L. Kelland, *Nat. Rev. Cancer* **2007**, *7*, 573; b) J. H. Schiller, D. Harrington, C. P. Belani, C. Langer, A. Sandler, J. Krook, J. Zhu, D. H. Johnson, *N. Engl. J. Med.* **2002**, *346*, 92.

[2] a) B. Stordal, N. Pavlakis, R. Davey, *Cancer Treat. Rev.* **2007**, *33*, 688; b) Z. H. Siddik, *Oncogene* **2003**, *22*, 7265.

[3] a) P. C. A. Bruijnincx, P. J. Sadler, *Curr. Opin. Chem. Biol.* **2008**, *12*, 197; b) R. W.-Y. Sun, D.-L. Ma, E. L.-M. Wong, C.-M. Che, *Dalton Trans.* **2007**, 4884; c) S. P. Fricker, *Dalton Trans.* **2007**, 4903; d) S. J. Lippard, *Nat. Chem. Biol.* **2006**, *2*, 504; e) H. B. Gray, *Proc. Natl. Acad. Sci. USA* **2003**, *100*, 3563; e) C. X. Zhang, S. J. Lippard, *Curr. Opin. Chem. Biol.* **2003**, *7*, 481; g) C. Orvig, M. J. Abrams, *Chem. Rev.* **1999**, *99*, 2201; M. J. Abrams, B. A. Murrer, *Science* **1993**, *261*, 725.

[4] P. J. Sadler, M. Nasr, V. L. Narayanan in *Platinum Coordination Complexes in Cancer Chemotherapy* (Eds.: M. P. Hacker, E. B. Douple, I. H. Krakoff), Martinus Nijhoff, Boston, **1984**, p. 209.

[5] a) V. Milacic, Q. P. Dou, *Coord. Chem. Rev.* **2009**, *253*, 1649; b) I. Ott, *Coord. Chem. Rev.* **2009**, *253*, 1670; c) A. Bindoli, M. P. Rigobello, G. Scutari, C. Gabbiani, A. Casini, L. Messori, *Coord. Chem. Rev.* **2009**, *253*, 1692; d) V. Milacic, D. Fregona, Q. P. Dou, *Histol. Histopathol.* **2008**, *23*, 101; e) X. Wang, Z. Guo, *Dalton Trans.* **2008**, 1521; f) I. Kostova, *Anti-Cancer Agents Med. Chem.* **2006**, *6*, 19; g) E. R. T. Tiekink, *Crit. Rev. Oncol. Hematol.* **2002**, *42*, 225; i) C. F. Shaw III, *Chem. Rev.* **1999**, *99*, 2589.

[6] For selected examples of cytotoxic gold(III) complexes reported from 2000 to 2008, see: a) C. Gabbiani, A. Casini, L. Messori, A. Guerri, M. A. Cinellu, G. Minghetti, M. Corsini, C. Rosani, P. Zanello, M. Arca, *Inorg. Chem.* **2008**, *47*, 2368; b) A. Casini, C. Hartinger, C. Gabbiani, E. Mini, P. J. Dyson, B. K. Keppler, L Messori, *J. Inorg. Biochem.* **2008**, *102*, 564; c) D. Saggioro, M. P. Rigobello, L. Paloschi, A. Folda, S. A. Moggach, S. Parsons, L. Ronconi, D. Fregona, A. Bindoli, *Chem. Biol.* **2007**, *14*, 1128; d) L. Engman, M. McNaughton, M. Gajewska, S. Kumar, A. Birmingham, G. Powis, *Anti-Cancer Drugs* **2006**, *17*, 539; e) Y. Omata, M. Folan, M. Shaw, R. L. Messer, P. E. Lockwood, D. Hobbs, S. Bouillaguet, H. Sano, J. B. Lewis, J. C. Wataha, *Toxicol. in Vitro* **2006**, *20*, 882; f) K. Palanichamy, A. C. Ontko, *Inorg. Chim. Acta* **2006**, *359*, 44; g) V. Milacic, D. Chen, L. Ronconi, K. R. Landis-Piwowar, D. Fregona, Q. P. Dou, *Cancer Res.* **2006**, *66*, 10478; h) P. Shi, Q. Jiang, J. Lin, Y. Zhao, L. Lin, Z. Guo, *J. Inorg. Biochem.* **2006**, *100*, 939; i) A. Casini, M. A. Cinellu, G. Minghetti, C. Gabbiani, M. Coronnello, E. Mini, L. Messori, *J. Med. Chem.* **2006**, *49*, 5524; j) P. Shi, Q. Jiang, Y. Zhao, Y. Zhang, J. Lin, L. Lin, J. Ding, Z. Guo, *J. Biol. Inorg. Chem.* **2006**, *11*, 745; k) L. Ronconi, C. Marzano, P. Zanello, M. Corsini, G. Miolo, C. Macca, A. Trevisan, D. Fregona, *J. Med. Chem.* **2006**, *49*, 1648; l) L. Giovagnini, L. Ronconi, D. Aldinucci, D. Lorenzon, S. Sitran, D. Fregona, *J. Med. Chem.* **2005**, *48*, 1588; m) L. Ronconi, L. Giovagnini, C. Marzano, F. Bettio, R. Graziani, G. Pilloni, D. Fregona, *Inorg. Chem.* **2005**, *44*, 1867; n) M. Coronnello, E. Mini, B. Caciagli, M. A. Cinellu, A. Bindoli, C. Gabbiani, L. Messori, *J. Med. Chem.* **2005**, *48*, 6761; o) L. Messori, G. Marcon, M. A. Cinellu, M. Coronnello, E. Mini, C. Gabbiani, P. Orioli, *Bioorg. Med. Chem.* **2004**, *12*, 6039; p) M. P. Rigobello, L. Messori, G. Marcon, M. A. Cinellu, M. Bragadin, A. Folda, G. Scutari, A. Bindoli, *J. Inorg. Biochem.* **2004**, *98*, 1634; q) T. Yang, C. Tu, J. Zhang, L. Lin, X. Zhang, Q. Liu, J. Ding, Q. Xu, Z. Guo, *Dalton Trans.* **2003**, 3419; r) C. H. A. Goss, W. Henderson, A. L. Wilkins, C. Evans, *J. Organomet. Chem.* **2003**, *679*, 194; s) J. J. Criado, J. L. Manzano, E. Rodriguez-Fernandez, *J. Inorg. Biochem.* **2003**, *96*, 311; t) D. Fan, C.-T. Yang, J. D. Ranford, P. F. Lee, J. J. Vittal, *Dalton Trans.* **2003**, 2680; u) G. Marcon, S. Carotti, M. Coronnello, L. Messori, E. Mini, P. Orioli, T. Mazzei, M. A. Cinellu, G. Minghetti, *J. Med. Chem.* **2002**, *45*, 1672; v) L. Messori, F. Abbate, G. Marcon, P. Orioli, M. Fontani, E. Mini, T. Mazzei, S. Carotti, T. O'Connell, P. Zanello, *J. Med. Chem.* **2000**, *43*, 3541; w) F. Abbate, P. Orioli, B. Bruni, G. Marcon, L. Messori, *Inorg. Chim. Acta* **2000**, *311*, 1.

[7] a) R. G. Buckley, A. M. Elsome, S. P. Fricker, G. R. Henderson, B. R. C. Theobald, R. V. Parish, B. P. Howe, L. R. Kelland, *J. Med. Chem.* **1996**, *39*, 5208; b) R. V. Parish, B. P. Howe, J. P. Wright, J. Mack, R. G. Pritchard, R. G. Buckley, A. M. Elsome, S. P. Fricker, *Inorg. Chem.* **1996**, *35*, 1659.

[8] C. K.-L. Li, R. W.-Y. Sun, S. C.-F. Kui, N. Zhu, C.-M. Che, *Chem. Eur. J.* **2006**, *12*, 5253.

[9] a) R. W.-Y. Sun, C.-M. Che, *Coord. Chem. Rev.* **2009**, *253*, 1682; b) Y. F. To, R. W.-Y. Sun, V. S.-F. Chan, Y. Chen, W.-Y. Yu, P. K.-H. Tam, C.-M. Che, C.-L. S. Lin, *Int. J. Cancer* **2009**, *124*, 1971; c) Y. Wang, Q.-Y. He, C.-M. Che, S. W. Tsao, R. W.-Y. Sun, J.-F. Chiu, *Biochem. Pharmacol.* **2008**, *75*, 1282; d) Y. Wang, Q.-Y. He, R. W.-Y. Sun, C.-M. Che, J.-F. Chiu, *Eur. J. Pharmacol.* **2007**, *554*, 113; e) C. T. Lum, Z. F. Yang, H. Y. Li, R. W.-Y. Sun, S. T. Fan, R. T. P. Poon, M. C. M. Lin, C.-M. Che, H. F. Kung, *Int. J. Cancer* **2006**, *118*, 1527; f) Y. Wang, Q.-Y. He, C.-M. Che, J.-F. Chiu, *Proteomics* **2006**,

6, 131; g) Y. Wang, Q.-Y. He, R. W.-Y. Sun, C.-M. Che, J.-F. Chiu, *Cancer Res.* **2005**, *65*, 11553; h) R. W.-Y. Sun, W.-Y. Yu, H. Sun, C.-M. Che, *ChemBioChem* **2004**, *5*, 1293; i) C.-M. Che, R. W.-Y. Sun, W.-Y. Yu, C.-B. Ko, N. Zhu, H. Sun, *Chem. Commun.* **2003**, 1718; j) K. H.-M. Chow, R. W.-Y. Sun, J. B. B. Lam, C. K.-L. Li, A. Xu, D.-L. Ma, R. Abagyan, Y. Wang, C.-M. Che. *Cancer Res.* **2010**, *70*, 329.

[10] a) D. Wang, S. J. Lippard, *Nat. Rev. Drug Discovery* **2005**, *4*, 307; b) P. M. Takahara, A. C. Rosenzweig, C. A. Frederick, S. J. Lippard, *Nature* **1995**, *377*, 649; c) G. Chu, *J. Biol. Chem.* **1994**, *269*, 787.

[11] J. S. Modica-Napolitano, J. R. Aprille, *Adv. Drug Delivery Rev.* **2001**, *49*, 63.

[12] V. R. Fantin, M. J. Berardi, L. Scorrano, S. J. Korsmeyer, P. Leder, *Cancer Cell* **2002**, *2*, 29.

[13] K. Koya, Y. Li, H. Wang, T. Ukai, N. Tatsuta, M. Kawakami, T. Shishido, L. B. Chen, *Cancer Res.* **1996**, *56*, 538.

[14] a) P. J. Barnard, S. J. Berners-Price, *Coord. Chem. Rev.* **2007**, *251*, 1889; b) M. J. McKeage, L. Maharaj, S. J. Berners-Price, *Coord. Chem. Rev.* **2002**, *232*, 127.

[15] S. J. Berners-Price, A. Filipovska, *Aust. J. Chem.* **2008**, *61*, 661.

[16] a) A. D. Adler, F. R. Longo, J. D. Finarelli, J. Goldmacher, J. Assour, L. Korsakoff, *J. Org. Chem.* **1967**, *32*, 476; b) J. S. Lindsey, H. C. Hsu, I. C. Schreiman, *Tetrahedron Lett.* **1986**, *27*, 931; c) D. Oulmi, P. Maillard, J. L. Guerquin-Kern, C. Huel, M. Momenteau, *J. Org. Chem.* **1995**, *60*, 1554; d) P. Maillard, J. L. Guerquin-Kern, C. Huel, M. Momenteau, *J. Org. Chem.* **1993**, *58*, 2774.

[17] a) E. B. Fleischer, A. Laszlo, *Inorg. Nucl. Chem. Lett.* **1969**, *5*, 373; b) M. E. Jamin, R. T. Iwamoto, *Inorg. Chim. Acta* **1978**, *27*, 135.

[18] Z. Abou-Gamra, A. Harriman, P. Neta, *J. Chem. Soc. Faraday Trans. 2* **1986**, *82*, 2337.

[19] T. Mosmann, *J. Immunol. Methods* **1983**, *65*, 55.

[20] a) E. J. Ngen, T. S. Daniels, R. S. Murthy, M. R. Detty, Y. You, *Bioorg. Med. Chem.* **2008**, *16*, 3171; b) D. Lahaye, K. Muthukumaran, C.-H. Hung, D. Gryko, J. S. Reboucas, I. Spasojevic, I. Batinic-Haberle, J. S. Lindsey, *Bioorg. Med. Chem.* **2007**, *15*, 7066; c) S. Banfi, E. Caruso, L. Buccafurni, V. Battini, S. Zazzaron, P. Barbieri, V. Orlandi, *J. Photochem. Photobiol. B* **2006**, *85*, 28; d) Y.-S. Kim, R. Song, D. H. Kim, M. J. Jun, Y. S. Sohn, *Bioorg. Med. Chem.* **2003**, *11*, 1753.

[21] M. J. McKeage, S. J. Berners-Price, P. Galettis, R. J. Bowen, W. Brouwer, L. Ding, L. Zhuang, B. C. Baguley, *Cancer Chemother. Pharmacol.* **2000**, *46*, 343.

[22] a) M. De Cesare, G. Pratesi, P. Perego, N. Carenini, S. Tinelli, L. Merlini, S. Penco, C. Pisano, F. Bucci, L. Vesci, S. Pace, F. Capocasa, P. Carminati, F. Zunino, *Cancer Res.* **2001**, *61*, 7189; b) Y. Liu, N. S. Ramamurthy, J. Marecek, H. M. Lee, J. L. Chen, M. E. Ryan, B. R. Rifkin, L. M. Golub, *Curr. Med. Chem.* **2001**, *8*, 243; c) A. Q. Siddiqui, C. Ballatore, D. McGuigan, E. De Clercq, J. Balzarini, *J. Med. Chem.* **1999**, *42*, 393.

[23] B. A. Desany, A. A. Alcasabas, J. B. Bachant, S. J. Elledge, *Genes Dev. Genes Develop.* **1998**, *12*, 2956.

[24] I. Herr, K. M. Debatin, *Blood* **2001**, *98*, 2603.

[25] C. V. Kumar, E. H. Asuncion, *J. Am. Chem. Soc.* **1993**, *115*, 8547.

[26] K. E. Reinert, *Biochim. Biophys. Acta* **1973**, *319*, 135.

[27] a) A. Siddiqui-Jain, C. L. Grand, D. J. Bearss, L. H. Hurley, *Proc. Natl. Acad. Sci. USA* **2002**, *99*, 11593; b) E. Izbicka, R. T. Wheelhouse, E. Raymond, K. K. Davidson, R. A. Lawrence, D. Sun, B. E. Windle, L. H. Hurley, D. D. Von Hoff, *Cancer Res.* **1999**, *59*, 639.

[28] T.-M. Ou, Y.-J. Lu, C. Zhang, Z.-S. Huang, X.-D. Wang, J.-H. Tan, Y. Chen, D.-L. Ma, K.-Y. Wong, J. C.-O. Tang, A. S.-C. Chan, L.-Q. Gu, *J. Med. Chem.* **2007**, *50*, 1465.

[29] L. F. Liu, *Annu. Rev. Biochem.* **1989**, *58*, 351.

[30] L. Hu, Z.-R. Li, Y. Li, J. Q, Y.-H. Ling, J.-D. Jiang, D. W. Boykin, *J. Med. Chem.* **2006**, *49*, 6273.

[31] A. Casini, C. Gabbiani, F. Sorrentino, M. P. Rigobello, A. Bindoli, T. J. Geldbach, A. Marrone, N. Re, C. G. Hartinger, P. J. Dyson, L. Messori, *J. Med. Chem.* **2008**, *51*, 6773.

[32] A. Mukherjee, A. D. Westwell, T. D. Bradshaw, M. F. G. Stevens, J. Carmichael, S. G. Martin, *Br. J. Cancer* **2005**, *92*, 350.

[33] S. Davis, M. J. Weiss, J. R. Wong, T. J. Lampidis, L. B. Chen, *J. Biol. Chem.* **1985**, *260*, 13844.

[34] E. Kimura, Y. Kurogi, T. Koike, M. Shionoya, Y. Iitaka, *J. Coord. Chem.* **1993**, *28*, 33.

[35] a) H.-Q. Liu, T.-C. Cheung, S.-M. Peng, C.-M. Che, *J. Chem. Soc. Chem. Commun.* **1995**, 1787; b) L. S. Hollis, S. J. Lippard, *J. Am. Chem. Soc.* **1983**, *105*, 4293.

[36] a) R. Vanyur, K. Heberger, I. Kovesdi, J. Jakus, *J. Photochem. Photobiol.* **2002**, *75*, 471; b) O. A. Raevsky, *J. Phys. Org. Chem.* **1997**, *10*, 405.

[37] a) M. B. Sevigny, C.-F. Li, M. Alas, M. Hughes-Fulford, *FEBS Lett.* **2006**, *580*, 6533; b) T. K. M. Shing, C. S. K. Kwong, A. W. C. Cheung, S. H.-L. Kok, Z. Yu, J. Li, C. H. K. Cheng, *J. Am. Chem. Soc.* **2004**, *126*, 15990.

[38] a) M. S. Deshpande, A. A. Kumbhar, A. S. Kumbhar, M. Kumbhakar, H. Pal, U. B. Sonawane, R. R. Joshi, *Bioconjugate Chem.* **2009**, *20*, 447; b) C.-M. Che, M. Yang, K.-H. Wong, H.-L. Chan, W. Lam, *Chem. Eur. J.* **1999**, *5*, 3350.

[39] D.-L. Ma, T. Y.-T. Shum, F. Zhang, C.-M. Che, M. Yang, *Chem. Commun.* **2005**, 4675.

[40] T. Sandalova, L. Zhong, Y. Lindqvist, A. Holmgren, G. Schneider, *Proc. Natl. Acad. Sci. USA* **2001**, *98*, 9533.

[41] A. G. Cox, K. K. Brown, E. S. J. Arner, M. B. Hampton, *Biochem. Pharmacol.* **2008**, *76*, 1097.

[42] J. E. Reynolds, T. Yang, L. Qian, J. D. Jenkinson, P. Zhou, A. Eastman, R. W. Craig, *Cancer Res.* **1994**, *54*, 6348.

[43] M. Galanski, V. B. Arion, M. A. Jakupec, B. K. Keppler, *Curr. Pharm. Des.* **2003**, *9*, 2078.

[44] G. M. Sheldrick, SHELXS-97, Program for the Solution of Crystal Structures, University of Göttingen, Göttingen (Germany), **1997**.

[45] A. Holmgren, *J. Biol. Chem.* **1977**, *252*, 4600.

[46] B.-L. Mau, G. Powis, *Biochem. Pharmacol.* **1992**, *43*, 1613.

[47] D. Suh, J. B. Chaires, *Bioorg. Med. Chem.* **1995**, *3*, 723.

[48] Gaussian 03, Revision B.05, M. J. Frisch, G. W. Trucks, H. B. Schlegel, G. E. Scuseria, M. A. Robb, J. R. Cheeseman, J. A. Montgomery, Jr., T. Vreven, K. N. Kudin, J. C. Burant, J. M. Millam, S. S. Iyengar, J. Tomasi, V. Barone, B. Mennucci, M. Cossi, G. Scalmani, N. Rega, G. A. Petersson, H. Nakatsuji, M. Hada, M. Ehara, K. Toyota, R. Fukuda, J. Hasegawa, M. Ishida, T. Nakajima, Y. Honda, O. Kitao, H. Nakai, M. Klene, X. Li, J. E. Knox, H. P. Hratchian, J. B. Cross, V. Bakken, C. Adamo, J. Jaramillo, R. Gomperts, R. E. Stratmann, O. Yazyev, A. J. Austin, R. Cammi, C. Pomelli, J. W. Ochterski, P. Y. Ayala, K. Morokuma, G. A. Voth, P. Salvador, J. J. Dannenberg, V. G. Zakrzewski, S. Dapprich, A. D. Daniels, M. C. Strain, O. Farkas, D. K. Malick, A. D. Rabuck, K. Raghavachari, J. B. Foresman, J. V. Ortiz, Q. Cui, A. G. Baboul, S. Clifford, J. Cioslowski, B. B. Stefanov, G. Liu, A. Liashenko, P. Piskorz, I. Komaromi, R. L. Martin, D. J. Fox, T. Keith, M. A. Al-Laham, C. Y. Peng, A. Nanayakkara, M. Challacombe, P. M. W. Gill, B. Johnson, W. Chen, M. W. Wong, C. Gonzalez, J. A. Pople, Gaussian, Inc., Wallingford CT, **2004**.

[49] a) P. J. Hay, W. R. Wadt, *J. Chem. Phys.* **1985**, *82*, 270; b) W. R. Wadt, P. J. Hay, *J. Chem. Phys.* **1985**, *82*, 284; c) P. J. Hay, W. R. Wadt, *J. Chem. Phys.* **1985**, *82*, 299.

[50] M. Totrov, R. Abagyan, *Proteins* **1997**, *29*, 215.

Received: September 5, 2009
Revised: December 15, 2009
Published online: February 16, 2010

